# MATERIAL DURABILITY IN WATER HAMMER SYSTEMS: STRENGTH, WEAR, AND SERVICE LIFE OF THE GIF² IMPULSE FLOW FORMER

Authors: Valerii Orlov[1]
[1] FLOW JET ENERGY LTD (Тел. (+47) 968 20 673; e-mail: flow.jet.energy@gmail.com)
Manuscript v6.1 – 17.02.2026 (EN)

## Abstract

The article presents a comprehensive materials science substantiation for the selection of structural materials for all main components of the Gravitational-Impulse Flow Former (GIF²) system [1–3]. The system operates under an extreme cyclic regime: pressure amplitude up to 15.2 MPa (150 atm), nominal impulse frequency of 2.39 Hz, local flow velocity up to 126 m/s, instantaneous flow rate up to 338 L/s [3]. Based on an analysis of the operating conditions and detailed design documentation [4–9], engineering calculations of strength, fatigue life [14, 15, 17], wear resistance [18–21], and service life were performed for 20 main system components (according to AISI and GOST/DSTU standards): the tank with a load-bearing secondary bottom (AISI 316) [4], pipelines and angle elbows (AISI 316) [4, 29], swing check valves (AISI 4340, AISI 9310, ceramic bearings (SiC, CeramicSpeed type) [5], two-stage spring pressure absorbers (AISI 4340, titanium VT6, 50KhFA) [6], Laval nozzle (40KhN2MA) [7], hydraulic seal (AISI 304) [8], accumulator-stabilizer (AISI 4340, reinforced polymer (PTFE) [2, 24, 25], and the nozzle assembly (Inconel 718) [9, 23]. A separate section is devoted to the engineering substantiation of the operability of swing check valves under cyclic water hammer conditions of 150 atm with a frequency of 2.39 Hz [5, 10–13, 17, 19, 20]. The calculation results confirm the achievement of the design service life of at least 15 years of continuous round-the-clock operation for all system components, except for the accumulator membrane, which is a replaceable element and requires periodic replacement [2, 24, 25]. The energy substantiation of the system's operability, including the energy concentration coefficient (KEP = 574) and conversion efficiency (η = 66.1%), is presented in [3].

**Keywords:** water hammer, fatigue strength, strength analysis, wear resistance, service life, AISI 316, AISI 4340, AISI 9310, titanium VT6, 51CrV4, SiC, DLC coating, swing check valve, gravitational-impulse integrator, Pelton nozzle, nozzle assembly needle, autonomous regulation, specific enthalpy of the module, energy concentration, KEP, Karni ϕ-index.

# 1. Introduction.

The Gravitational-Impulse Flow Former (GIF²) system is an innovative hydraulic device that uses controlled water hammer for the temporal concentration of energy from a low-head gravitational flow (static head 0.65–1.5 m) [1–3]. Classical water hammer engineering considers transient processes as parasitic phenomena to be avoided [10–12]. In contrast, GIF² deliberately generates them, which imposes fundamentally new requirements on structural materials [13].

The dynamics of valve closure and the formation of water hammer are described in [2] and analyzed in detail in [3] based on numerical simulation considering fluid-structure interaction (FSI) [13]. In this work, the peak pressure values (up to 15.2 MPa) and characteristic valve closure times (0.765–1.34 ms) are adopted as initial design parameters. These values are considered a conservative estimate of the upper load limit, providing a sufficient safety margin for structural elements.

The GIF² system is a self-oscillating hydrodynamic system, where the frequency and cycle are shaped by the internal dynamics of the valves, while the working fluid flow remains the energy source. The formation of high pressures (up to 150 atm) is due to water hammer processes, rather than energy generation within the system.

A detailed energy analysis of the GIF² system is given in [3]. In the nominal cycle, the system converts gravitational work:

$$\mathbf{Egrav = \rho g h V tot \approx 1{,}96\ kJ} \quad (1)$$

per cycle into the kinetic energy of the flow, which during water hammer is transformed into the enthalpy work potential (P−Patm)V [35] of the main module:

$$\mathbf{Hmax = (P - Patm) Vmod \approx 1704\ kJ}. \quad (2)$$

This is made possible by temporal energy concentration (accumulation over ~0.4 s and release over ~2 ms), the Joukowsky transformation ($\Delta P = \rho c \Delta v$, *c* = 910 m/s), and internal energy recovery through the rarefaction phase ($P \approx -0.8$ atm), which provides ~38.5 kJ for accelerating the next cycle.

The energy concentration coefficient is defined as:

$$\mathbf{KEPcycle} = \frac{\mathbf{Hdel}}{\mathbf{Egrav}} \approx \mathbf{574}, \quad (3)$$

which does not contradict the law of energy conservation, since *KEP* is a measure of temporal and spatial concentration, not efficiency [3]. The conversion efficiency of the module's enthalpy into delivered work is:

$$\eta = \frac{\mathbf{Hdel}}{\mathbf{Hmax}} \approx \mathbf{66{,}1}\%, \quad (4)$$

fully consistent with the energy balance.

The initial parameters for the calculations (geometric dimensions, materials, operating modes) are adopted according to the design documentation [4–9] and patents [1, 2]. The dynamic characteristics of the transient processes (pressure, flow velocity, valve closure time) are obtained based on numerical simulation considering fluid-structure interaction (FSI), the results of which are detailed in a separate work devoted to the energy analysis of the GIF² system [3]. In this article, these parameters are used as input data for engineering calculations of strength, fatigue life, wear resistance, and service life, which are performed according to the fundamental principles outlined in [10–39].

These parameters define the material requirements: the ability to withstand cyclic loads up to 150 atm at a frequency of 2.39 Hz; erosion resistance at flow velocities up to 300 m/s (taken as a conservative design limit for strength assessment of components, in particular the drain Laval nozzle), and 126 m/s (nominal mode at the nozzle assembly outlet); as well as ensuring a service life of at least 15 years under the specified operating conditions.

In the nominal operating mode of the system, the maximum water hammer pressure is 120.5 atm (12.2 MPa) at an impulse frequency of 2.39 Hz [3]. In the strength and service life calculations, a **conservative value of 150 atm (15.2 MPa)** is used, which provides an additional safety margin for all structural elements.

Special attention in this work is given to the swing check valves (V2, V4, V7), since they are subjected to the most intense cyclic loads and raise the most doubts among specialists regarding their operability. Section 4.3 provides a detailed engineering substantiation that dispels these doubts.

The aim of this work is to provide a scientific substantiation of the material selection for all main elements of the GIF² system subjected to extreme cyclic loads, considering their operating modes and conditions, to ensure maximum strength and durability (design service life ≥ 15 years of continuous round-the-clock operation). The work is based on numerical simulation data [3], patent data [1, 2], and detailed design documentation [4–9].

# 2. Design and Operating Principle of the GIF² System

## 2.1. General System Layout.

The GIF² (Gravity Impulse Flow Former) system is a gravitational-impulse flow integrator that converts a low-energy gravitational flow into a high-pressure quasi-continuous fluid jet [1, 2]. The system design includes the following main components (numbering corresponds to the patent description [2] and design documentation [4–9]):

A schematic diagram of the GIF² system is shown in Fig. 1 [2].

**External flow source – tank R1 with a load-bearing secondary bottom:**

- R1 – external source tank, material AISI 316, wall thickness 8 mm, diameter 1700 mm, cylindrical part height 1300 mm [4].
- G – load-bearing horizontal secondary bottom, located at a height of 300 mm from point 7.1, gap between the secondary bottom and side walls 10 mm, mounted on 5 vertical guides [4].
- 7.1 – opening with a diameter of 245 mm in the center of the conical bottom for connection to elbow A1 [4].
- S – industrial automatic air vent.
- 3 – water intake pipe (diameter 506 mm).
- 2 – pipe for initial filling (diameter 500 mm).

**Pipeline system:**

- 1 – inclined supply pipeline ($L_1$ = 1.7 m, $D_{int}$ = 245 mm, AISI 316) [4].
- 3 – horizontal working pipeline ($L_3$ = 3.0 m, $D_{int}$ = 245 mm, AISI 316) [4].
- 5 – discharge pipeline ($L_5$ = 4.7 m, AISI 316) [4].
- 9 – horizontal pressure pipeline ($L_9$ = 3.85 m, AISI 316) [4].
- 8 – angle elbow 15° (AISI 316) [4].
- 13 – angle elbow 75° (AISI 316) [4].
- 14 – angle elbow 90° (AISI 316) [4].
- 18 – angle elbow 51° (AISI 316) [4].
- 19 – angle elbow 39° (AISI 316) [4].
- A1 – connecting elbow (39°, AISI 316) with Inconel 718 flange [4].

**Valve assembly:**

- V2 (V13) – swing check interrupter valve (DN250 PN250) [5].
- V4 (V17) – impact swing check valve (DN250 PN250) [5].
- V7 (V16) – discharge swing check valve (DN250 PN250) [5].

**Energy dissipation system (discharge pipeline 5):**

- SL-16 – Laval nozzle (40KhN2MA, AISI 4340) [7].
- GZ-6 – hydraulic seal with inclined discharge (AISI 304) [8].

**Shock wave damping system:**

- 17 – spring-type hydraulic impulse pressure amplitude damper (supply pipeline) [6].
- 15 – spring-type hydraulic impulse pressure amplitude damper (discharge pipeline) [6].

**Stabilization and jet formation system:**

- 10 – transit diaphragm accumulator-stabilizer (AISI 4340, reinforced PTFE diaphragm) [2].
- 12 – nozzle element (Pelton turbine nozzle, Inconel 718) [9].

## 2.2. Tank with Load-Bearing Secondary Bottom (R1, G).

The tank R1 is a key element of the system, ensuring stable fluid supply and participating in the damping of shock waves. According to technical specification No. 4 [4]:

**Geometric parameters:**

- Tank diameter: D = 1700 mm.
- Cylindrical part height: $h_1$ = 1300 mm.
- Conical bottom height: $h_2$ = 200 mm.
- Wall thickness: $\delta$ = 8 mm.

- Opening diameter in the conical bottom (point 7.1): $D_{op}$= 245 mm.
- Distance from point 7.1 to the secondary bottom: hG = 300 mm.
- Gap between the secondary bottom and the wall: Δ = 10 mm.

**Functional purpose of the secondary bottom G:**

*1. Hydrodynamic separator* – separates the air cushion in the upper part of the tank from the fluid entering the supply pipeline.

*2. Pressure reference plane* – creates a clear fixed elevation mark for gravitational head.

*3. Shock wave damper* – reduces the amplitude of shock waves through elastic deformation and interaction with the fluid column [13].

*4. Guiding structure* – 5 vertical guides ensure a stable position of the secondary bottom.

**Fig. 1** – Schematic diagram of the Gravitational-Impulse Flow Former (GIF²), developed in [2].

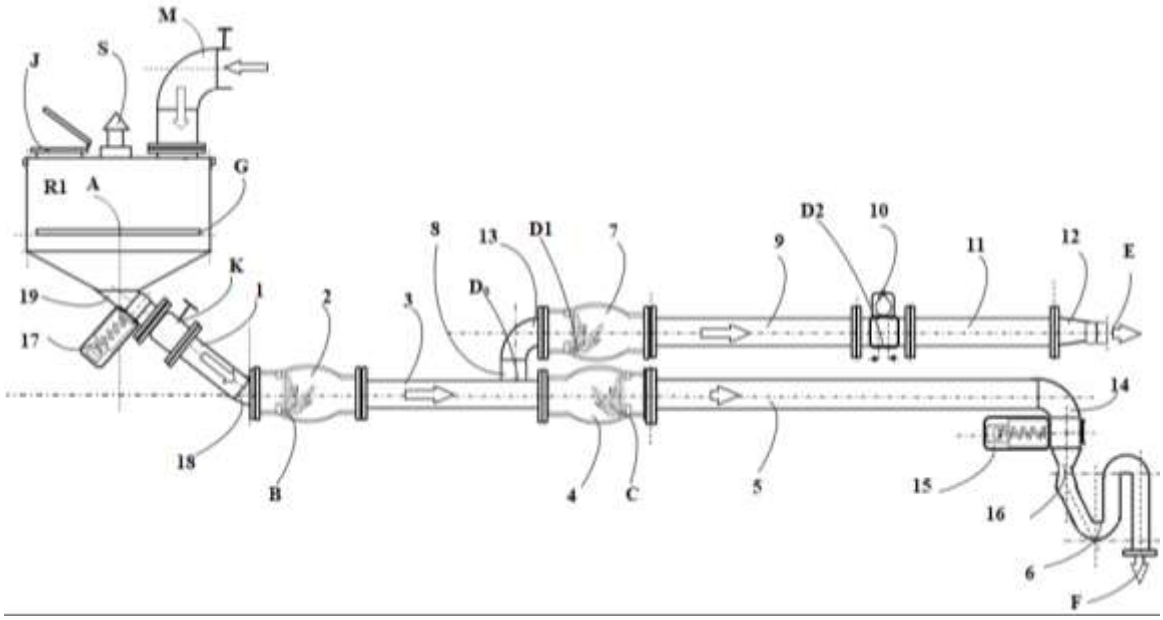


**2.3. Swing Check Valves V2, V4, V7.**

The valves are manufactured according to a unified design scheme DN250 PN250 with the following parameters [5]:

**Table 1.**

| Element | Material | Dimensions | Features | Service Life |
|---|---|---|---|---|
| Valve body | AISI 4340 | Wall 60 mm, length 600–900 mm | Nickel plating of internal surface | ≥ 15 years |
| Conical disc | AISI 9310 | ⌀323.8 mm, mass 4 kg | Carburizing, DLC coating [20] | ≥ 5 years |
| Rotating shaft | AISI 9310 | ⌀36 mm | Carburizing | ≥ 15 years |
| Bearing | CeramicSpeed | 36×45×50 mm | Ceramic | ≥ 15 years |
| Seat | SiC + DLC | Passage diameter 238 mm | Silicon carbide [20] | ≥ 25 years |
| Flange | Inconel 718 | Thickness 40 mm, 12×M27 | Superalloy [23] | ≥ 100 years |
| Gasket | FKM (Viton) | 4 mm | – | ≥ 8 years |

**2.4. Spring Pressure Absorbers (Items 17 and 15).**

The absorbers are manufactured according to a two-stage scheme with the following parameters [6]:

**Table 2.**

| Parameter | Absorber 17 (supply) | Absorber 15 (discharge) |
|---|---|---|
| Final pressure | 1.8 atm | 1.087 atm |
| Service life | 950 million cycles (20 years) | 800 million cycles (17 years) |
| Spring stiffness 1 | 3.5 MN/m | 3.62 MN/m |
| Spring stiffness 2 | 11.8 MN/m | 11.7 MN/m |
| Spring material | 50KhFA (51CrV4) [30] | 50KhFA (51CrV4) [30] |
| Diaphragm material | Titanium VT6 (Grade 5) [16] | Titanium VT6 (Grade 5) [16] |
| Diaphragm coating | $Al_2O_3$ (100–150 μm) | $Al_2O_3$ (100–150 μm) |
| Housing material | 40KhN2MA (AISI 4340) [16] | 40KhN2MA (AISI 4340) [16] |

### 2.5. Energy Dissipation System (SL-16 and GZ-6).

**Laval–Venturi type nozzle (SL-16) [7]:**

A throttling element designed for controlled deceleration of the small impulse module flow with intensification of its kinetic energy dissipation.

**Purpose:** conversion of the kinetic energy of the small module into heat through turbulent, viscous and cavitation losses, as well as the formation of hydraulic resistance that limits the flow rate through the drain branch.

**Design:** Laval–Venturi type throttling nozzle consisting of a converging section, a small throat, and a subsequent abrupt expansion. This geometry provides:

- local increase of velocity and pressure gradients in the throat;
- initiation of cavitation and turbulent processes;
- intense jet breakup upon sudden expansion with formation of vortex structures and energy dissipation.

**Main geometric parameters:**

- inlet channel diameter: ~4–6 mm (effective jet diameter before the throat; a sharp contraction from pipeline 5 (Ø245 mm) to a diameter of ~5 mm occurs immediately before the nozzle);
- throat diameter: 0.8 mm;
- outlet diameter after expansion: ~3 mm;
- convergence angle: ~30°;
- expansion: abrupt (stepwise), equivalent angle ~90°;
- overall length: ~10 mm..

**Hydrodynamic parameters:**

- low rate: $Q \approx 0.00062$ $m^3/s$;
- haracteristic inlet velocity: $v \approx 28.1$ m/s;
- local velocity in the throat can reach high values due to throttling and flow unsteadiness;
- the value $v \approx 300$ m/s is taken as a design limit for assessing material strength and erosion resistance and is not the average operating flow velocity.

**Energy characteristics:**

- small module energy: ~3.3 kJ per cycle;
- dissipation efficiency: ~75% in the nozzle;
- the remaining energy is dissipated in the hydraulic seal.

**Material:** 40XH2MA (AISI 4340), heat-treated to HRC 32–36 [16], providing sufficient fatigue strength and resistance to cavitation-erosion wear.

**Hydraulic seal with inclined drain (HZ-6) [8]:**

A volumetric hydraulic element designed for final dissipation of the small module energy and for providing a time spread of its release.

**Purpose:**

- final damping of the residual kinetic energy of the flow
- preventing air suction into the system;
- creating a time delay for the small module release (not more than ~0.35 s).

**Operating principle:** After passing through the throttling nozzle, the flow loses coherence, becomes turbulent-cavitating and enters the hydraulic seal volume. Due to the large volume and change of flow direction, the following occurs:

- further reduction of flow velocity to values <1 m/s;
- energy dissipation through mixing, turbulence and viscous losses;
- gradual fluid release, which determines the duration of the process..

**Main parameters:**

- drain pipe inclination angle: ~65°;
- immersion depth: ≥150 mm;
- reservoir volume: ≥100 L;
- characteristic outlet velocity: ≤0.5–1 m/s.

**Material:** AISI 304 (pipe and reservoir) [16].

**Functional integration of SL-16 and HZ-6:**

The SL-16 nozzle and the HZ-6 hydraulic seal form a single dissipation system in which:

- he nozzle performs local throttling and primary energy conversion;
- the hydraulic seal provides volumetric dissipation and time stabilisation of the process;

he total energy of the small module (~3.3 kJ per cycle) is completely dissipated without affecting the main energy channel of the system.

This approach minimises energy losses (≈0.29% of the main module energy) while ensuring stable synchronisation and hydraulic isolation of the system.

**2.6. Nozzle Assembly (Item 12).**

The nozzle assembly is manufactured as a Pelton hydraulic turbine nozzle with a movable needle and a spring for autonomous flow regulation [9]:

**Geometric parameters:**

- Inlet diameter: 245 mm.
- Outlet orifice diameter (point E): 58.4 mm (tolerance ±0.1 mm).
- Flow rate: 338 L/s.
- Head: (equivalent hydraulic head) 810.6 m) 810.6 m.
- Outlet velocity: 126.11 m/s.
- Inlet pressure: 78.48 atm (7.96 MPa).

**Structural elements:**

- Body: AISI 316, wall thickness 5 mm [16]
- Needle: conical, material Inconel 718 with DLC coating [20, 23], diameter varies in the range of 56–58.4 mm, length of the conical part 50–100 mm, roughness $Ra \leq 0.8$ μm.
- Spring: AISI 302 [30], stiffness k = 115775 N/m, wire diameter 5.84 mm, mean diameter 60 mm, number of coils ≈6.73.
- Sealing: FKM (Viton) gasket, RTJ type [27], thickness 2–3 mm.

**Operating principle:**

The needle and spring operate automatically, regulating the flow without external actuators. The needle changes its position under the influence of flow pressure and spring elasticity, providing autonomous dynamic regulation of the water jet. This allows adapting the outlet orifice geometry to the energy state (enthalpy and velocity) of each impulse module [3].

**2.7. System Operating Principle.**

The operating cycle of the GIF² system consists of five main stages [2, 3]:

**Stage 1: Preparation and Start-up**

- The system is completely filled with water through the pipe (2) until a continuous outflow without gas inclusions appears through the air vent S.
- The interrupter valve V2 is open, the discharge valve V7 is closed, the impact valve V4 is open.
- A continuous flow from the tank R1 passes through the secondary bottom G and elbow A1 into the supply pipeline (1).

**Stage 2: Control Water Hammer and Formation of the Minor Module.**

- The flow reaches the impact valve V4, which closes sharply under the action of hydrodynamic pressure.
- A control water hammer with amplitude $\Delta P = \rho c \Delta v$ occurs [10–12]. (5)
- The minor control module (0.26 L in nominal mode) is directed into the discharge pipeline (5).
- The energy of the minor module (~3.3 kJ) is completely dissipated as it passes through the Laval nozzle SL-16 [7] and the hydraulic seal GZ-6 [8].

**Stage 3: Synchronizing Water Hammer and Formation of the Main Module.**

- The shock wave propagates upstream, opens the discharge valve V7 and sharply closes the interrupter valve V2.
- A synchronizing water hammer occurs, which forms the main impulse module with a volume of $V$mod= 141.3 L between the closed valves V2 and V4.
- The module is characterized by a high enthalpy state:

$$H\text{max} = (P - P\text{atm}) \cdot V\text{mod} \approx 1704 \text{ kJ [3]}. \quad (6)$$

- The shock wave reaches the tank R1, where it is damped by the secondary bottom G and the spring damper (17) [6].

**Stage 4: Transport and Stabilization.**

- The main module passes through the open discharge valve V7 into the pressure pipeline (9).
- After the module passes, valve V7 closes.
- In the working pipeline (3), a rarefaction phase occurs — the gauge pressure decreases to ≈ −0.8 atm, which corresponds to an absolute pressure of ≈ 0.2 atm. This value is close to the saturated vapour pressure of water at the operating temperature, which approaches the saturated vapour pressure of water at the operating temperature and may initiate controlled cavitation phenomena
- The module enters the accumulator-stabilizer (10), where its pressure is stabilized from 88.7 atm to 78.48 atm [2].

**Stage 5: Jet Formation.**

- The stabilised module enters the nozzle element (12), where its enthalpy is converted into jet kinetic energy [9] according to the Bernoulli equation for compressible flow.
- The jet velocity at the outlet reaches $v_{jet} \approx 126$ m/s.
- Due to phase overlap (up to 36%), the next module begins to form before the completion of the previous one's discharge, ensuring quasi-continuity of the jet [3].

# 3. Analysis of Operating Conditions and Material Selection Criteria.

Based on the data presented in the article [3], the patent description [2], and the design documentation [4–9], the key factors affecting materials are identified:

**Table 3. Load parameters of the GIF² system.**

| Parameter | Value | Note |
|---|---|---|
| Maximum operating pressure | 150 atm (15.2 MPa) | Water hammer [3] |
| Effective wave velocity | 910 m/s | Considering FSI and gas content [3, 13] |
| Nominal impulse frequency | 2.39 Hz | Period 0.418 s [3] |
| Flow rate through the system | 338 L/s | Design [4] |
| Flow velocity (nominal) | 13.42 m/s | Before water hammer [3] |
| Velocity in the Laval nozzle throat | 300 m/s | The maximum [7] is taken as a design limit for strength assessment |
| Jet velocity at the outlet | 126 m/s | Pelton nozzle [9] |
| Valve V4 closure time | 1.34 ms | Nominal mode [3] |
| Valve V2 closure time | 0.765 ms | Nominal mode [3] |
| Operating temperature | 5–150°C | Working medium – water |

**Failure mechanisms:**

*1.* ***Fatigue*** – the main mechanism for bodies, pipelines, the tank, and valve elements under cyclic loads [14, 15].

*2.* ***Abrasive and erosive wear –*** high-velocity fluid flow leads to erosion of valve seats, discs, and internal surfaces [21].

*3.* ***Contact fatigue and galling –*** for friction pairs (shaft-bushing, disc-seat) under high contact stresses [18, 19].

*4.* ***Corrosion resistance*** – the working medium is water with dissolved oxygen [22].

# 4. Substantiation of Material Selection.

## 4.1. Main Components and Materials.

Based on the above criteria, patent data [1, 2], technical specification [4], and design documentation [5–9], a consolidated material nomenclature has been formed.

**Table 4. Main components and materials of the GIF² integrator.**

| No. | Component | Item | Material | Standard | $\sigma_{UTS}$, MPa | Service Life, years |
|---|---|---|---|---|---|---|
| 1 | Tank R1 (body) | R1 | AISI 316 [16] | EN 10088 | 500 | ≥ 20 |
| 2 | Secondary bottom G | G | AISI 316 [16] | EN 10088 | 500 | ≥ 20 |
| 3 | Elbow A1 | A1 | AISI 316 [16] | EN 10088 | 500 | ≥ 20 |
| 4 | Elbow A1 flange | – | Inconel 718 [23] | AMS 5662 | 1300 | ≥ 35 |
| 5 | Pipelines | 1,3,5,9 | AISI 316 [16] | EN 10216-5 [29] | 500 | ≥ 20 |
| 6 | Angle elbows | 8,13,14,18,19 | AISI 316 [16] | EN 10216-5 [29] | 500 | ≥ 20 |
| 7 | Valve body | V2,V4,V7 | AISI 4340 + Ni [16] | ASTM A829 | 1080 | ≥ 15 |
| 8 | Valve disc | V2,V4,V7 | AISI 9310 + DLC [16, 20] | AMS 6265 | 1080 | ≥ 5 |
| 9 | Valve seat | V2,V4,V7 | SiC (base) with DLC coating [20] | ISO 21223 | 1000 | ≥ 25 |
| 10 | Rotating shaft | V2,V4,V7 | AISI 9310 [16] | AMS 6265 | 1080 | ≥ 15 |
| 11 | Bearing (support) | V2,V4,V7 | Ceramic bearings ($Si_3N_4$) [33] | ISO 26602 | 800 | ≥ 15 |
| 12 | Valve flange | V2,V4,V7 | Inconel 718 [23] | AMS 5662 | 1300 | ≥ 35 |
| 13 | Absorber 17 body | 17 | AISI 4340 [16] | ASTM A829 | 850 | ≥ 20 |

| No. | Component | Item | Material | Standard | $\sigma_{UTS}$, MPa | Service Life, years |
|---|---|---|---|---|---|---|
| 14 | Absorber 15 body | 15 | AISI 4340 [16] | ASTM A829 | 850 | ≥ 17 |
| 15 | Absorber diaphragm | 17,15 | Titanium VT6 (Grade 5) [16] | ASTM B348 | 950 | ≥ 20 |
| 16 | Absorber springs | 17,15 | 50KhFA (51CrV4) [30] | EN 10083-3 [30] | 1600 | ≥ 68 |
| 17 | Laval nozzle | SL-16 | 40KhN2MA (AISI 4340) [16] | ASTM A829 | 1080 | ≥ 20 |
| 18 | Hydraulic seal (pipe) | GZ-6 | AISI 304 [16] | EN 10088 | 520 | ≥ 15 |
| 19 | Hydraulic seal (tank) | GZ-6 | AISI 304 [16] | EN 10088 | 520 | ≥ 15 |
| 20 | Accumulator (body) | 10 | AISI 4340 [16] | ASTM A829 | 850 | ≥ 20 |
| 21 | Accumulator diaphragm | 10 | Reinforced PTFE (composite with textile or metal framework) [24, 25] | ISO 13000-1 [24] | 30 | ≥ 11 |
| 22 | Nozzle assembly (body) | 12 | AISI 316 [16] | EN 10088 | 500 | ≥ 15 |
| 23 | Nozzle assembly needle | 12 | Inconel 718 + DLC [20, 23] | AMS 5662 | 1300 | ≥ 15 |
| 24 | Nozzle assembly spring | 12 | AISI 302 [30] | ASTM A313 | 860 | ≥ 15 |
| 25 | Gasket (RTJ) | 12 | FKM (Viton) [27] | ASTM D1418 | – | ≥ 8 |
| 26 | Stop V2, V7 | V2,V7 | Stellite 6 (hardfacing) | ASTM F75 | 900 | ≥ 29 |
| 27 | Stop V4 | V4 | Inconel 718 | AMS 5662 | 1300 | > 25 |
| 28 | Shaft V2, V7 | V2,V7 | AISI 9310 (increased diameter) | AMS 6265 | 1080 | ≥ 25 |
| 29 | Bearings | V2,V4,V7 | Ceramic bearings ($Si_3N_4$) [33] | ISO 26602 | 800 | > 25* |

*Bearings do not experience impact load; service life is determined by wear from rotation.

### 4.2. Key Materials and Their Substantiation

**Table 5.**

| Material | Application | Substantiation |
|---|---|---|
| AISI 316 | Tank, pipelines, elbows | High corrosion resistance [22], excellent weldability, material unification [16] |
| AISI 4340 | Valve bodies, absorbers, accumulator | High-strength steel ($\sigma_{0.2}$ = 850 MPa), optimal combination of strength and toughness after heat treatment (quenching + tempering) [16] |
| AISI 9310 | Valve discs and shafts (high contact endurance under impact loads) | Nickel-chromium-molybdenum steel with high nickel content; after carburizing – surface hardness 58–62 HRC with a tough core [16] |
| SiC + DLC | Valve seats (resistance to cavitation erosion) | Silicon carbide (hardness >2500 HV) with diamond-like coating (coefficient of friction 0.05–0.1) [20] |
| CeramicSpeed | Valve bearings | $Si_3N_4$ ceramic, operation without lubrication, service life $>10^8$ cycles |

| Material | Application | Substantiation |
|---|---|---|
| Titanium VT6 | Absorber diaphragms | High strength (950 MPa), corrosion resistance, fatigue strength [16] |
| 50KhFA (51CrV4) | Absorber springs operating in the elastic deformation range | Specialized spring steel, tensile strength 1600 MPa, service life >$10^9$ cycles [30, 31] |
| Inconel 718 | Nozzle assembly, flanges | Nickel superalloy, resistance to erosion and corrosion, $\sigma_{0.2}$= 1030 MPa [23] |

### 4.3. Swing Check Valves: Detailed Analysis.

The valves V2, V4, V7 are the most critical elements of the system, as they are subjected to the most intense cyclic loads (150 atm, 2.39 Hz) and directly form the impulse modules. Their design is based on the following principles:

4.3.1. The "No Pockets" Principle.

Typical industrial valves have internal cavities, gaps, threaded connections that protrude into the flow path. These "pockets" are stress concentrators and zones for gas bubble accumulation. During a 150 atm water hammer, they act as local repeated impulse compression of micro-volumes of liquid, initiating cavitation erosion and fatigue cracks [10–13].

In the GIF² valves, all pockets have been deliberately eliminated [5]:

- Minimum body depth (absence of deep cavities).
- Smooth internal transitions without sharp corners.
- Absence of protruding elements in the flow path.
- The disc fits tightly against the seat without gaps.

This is not just a valve – it is a valve functionally equivalent to a hydraulically smooth channel, where the flow encounters no obstacles, and the internal geometry is optimised to minimise hydraulic losses and eliminate stagnation zones; the elimination of local low-pressure zones also minimises cavitation initiation.

#### 4.3.2. Comparison with Typical Industrial Valves.

**Table 6.**

| Parameter | Typical Industrial Valve DN250 PN250 | GIF² Valve DN250 PN250 [5] |
|---|---|---|
| Internal geometry | Pockets, gaps, threaded protrusions present | No pockets, smooth transitions |
| Wall thickness | 30–40 mm | 60 mm |
| Body material | Carbon steel (St37, St52) | AISI 4340 ($\sigma_{0.2}$ = 850 MPa) [16] |
| Protective coating | Paint | Nickel plating / chromium plating |
| Disc | Cast iron, stainless steel | AISI 9310 + DLC (carburizing, HRC 58–62) [16, 20] |
| Seat | Stainless steel, bronze | SiC + DLC (hardness >2500 HV) [20] |
| Bearings | Steel (require lubrication) | Ceramic (operation without lubrication) |
| Service life at 150 atm, 2 Hz | 2–5 years | ≥ 15 years |

#### 4.3.3. Key Design Parameters. Valve Closure Time: Substantiation of Realism.

**Table 7.**

| Parameter | Value | Significance |
|---|---|---|
| Body safety factor | *n* = 3.5 | At 150 atm, stress is 3.5 times lower than the yield strength [17] |
| Seat working surface hardness | >2500 HV | 5–10 times higher than steel counterparts [20] |
| Coefficient of friction in the disc- | 0.05–0.1 | 3–5 times lower than steel-on-steel [18, 20] |

| Parameter | Value | Significance |
|---|---|---|
| seat pair | | |
| Calculated wear over 15 years | 0.088 mm | 10 times less than permissible [19] |
| Bearing service life | $>10^8$ cycles | Corresponds to >30 years of continuous operation |

The valve closure times obtained from FSI modeling [3] are:

- V4 (impact valve) – 1.34 ms;
- V2 (interrupter valve) – 0.765 ms.

Such values are a conservative upper estimate and are achievable due to the following factors:

1. Driving force of closure. The valve discs are accelerated not by springs but by the fluid flow itself and/or the directed influence of the shock wave front after the water hammer, which ensures high closure/opening velocities. This principle is characteristic of hydraulic systems with controlled transient processes [10–13].
2. Small rotation angle (37° for V4, 52° for V2) and optimized flow path geometry minimize the disc travel distance.
3. FSI modeling [3] accounts for structural elasticity and fluid compressibility, allowing realistic dynamic characteristics to be obtained.
4. Even if the actual closure times are 2–3 times longer (which is possible due to manufacturing tolerances), this would only reduce the peak loads on the valve elements, thereby increasing the actual service life. Thus, using the calculated values of 0.765 ms and 1.34 ms provides a conservative safety margin.
5. Calculation of closure time. Valve closure times are the determining parameters that shape the intensity of the water hammer, the spectrum of pressure oscillations, and the level of dynamic loads on structural elements. For impulse hydraulic systems of the GIF² type, the closure process is determined by the unsteady interaction of the fluid flow and the inertial characteristics of the moving elements, which is consistent with classical approaches to the theory of water hammer and valve dynamics [12, 36–39].

**Geometry and Kinematics of Motion.**

The valve discs rotate about an axis located in the lower part of the body. Closure occurs against gravity:

- for V2, V7: $\Delta\theta = 52° = 0.908$ rad.
- for V4: $\Delta\theta = 37° = 0.646$ rad.

The small rotation angle is a fundamental design feature that ensures high valve responsiveness.

**Dynamic Model of Motion.**

The motion of the disc is described by the rotational motion equation considering hydrodynamic interaction:

$$I_{eff} \cdot \ddot{\theta} = M_{hyd(\theta, t)} - M_{res(\theta, \dot{\theta})} \quad (7)$$

where:

$I_{eff} = I + I_{fluid}$ - — effective moment of inertia considering the added mass of the fluid [12, 37];

$M_{hyd}$ - hydrodynamic moment from the flow and pressure waves;

$M_{res}$ - total resisting moment (hydrodynamic drag + friction).

**Estimation of Effective Moment of Inertia.**

For the disc:

$$I = \frac{1}{2} m \left(\frac{D}{2}\right)^2 = 0.0525 \ \mathbf{kg \cdot m^2}. \quad (8)$$

Considering the added mass of the fluid, which for disc valves can increase the moment of inertia by 3–6 times [37]: $\mathbf{I_{eff} = (0.15…0.30)\ kg \cdot m^2}$.

In the calculations, the following is adopted: $\mathbf{I_{eff} \approx 0.20\ kg \cdot m^2}$ (average value from the range 0.15–0.30 kg·m²).

**Estimation of Driving Moment.**

The hydrodynamic moment is formed not by the full static pressure, but by the effective part that is converted into motion. According to the models proposed in [12], the driving moment is proportional to the disc area and the pressure differential, but considering an efficiency coefficient:

$$\mathbf{M_{hyd} \approx \eta \cdot \Delta P_{max} \cdot A \cdot R} \quad (9)$$

where:

- $\eta = 0.05…0.15$ — efficiency coefficient of impulse transfer [12];
- Pmax= 15.2 MPa;
- $A = 0.0824$ m²;
- $R = 0.16$ m.

Taking $\eta = 0.1$ (conservative estimate):

$M_{hyd} \approx 2.0 \cdot 10^4$ N·m.

**Estimation of Angular Acceleration:**

$$\mathbf{\alpha = M_{hyd} / I_{eff} \approx 2.0 \cdot 10^4 / 0.20 \approx 1.0 \cdot 10^5\ rad/s^2.} \quad (10)$$

**Characteristic Closure Time:**

Characteristic Closure Time:

To estimate the order of magnitude, the integral form of motion is used: $t = \sqrt{\frac{2\theta}{\alpha}}$. (11)

- For V2, V7: *t* ~ 4.3 ms.
- For V4: *t* ~ 3.6 ms.

These values correspond to a quasi-static estimate.

**Table 7.1. Comparison with FSI Modeling.**

| Parameter | Analytical Estimate | FSI Modeling Data [3] |
|---|---|---|
| Closure time V2, V7 | ~4.3 ms | 0.765 ms |
| Closure time V4 | ~3.6 ms | 1.34 ms |

The analytical model gives an upper estimate of the closing time because it does not account for the impulse nature of the loading and the peak dP/dt during the passage of the water hammer front.

To verify the results of the FSI modeling [3], an analytical estimate of the closure time of valve V4 was performed for the start-up mode (P = 2.39 MPa, U = 2.66 m/s), which corresponds to the conditions of the first system start-up. Calculation using the rotational motion equation of the disc (formulas (7)–(11)) yields a value of *t* ≈ 1.7 ms. For the nominal mode, when after the rarefaction phase (–0.8 atm) the flow velocity reaches 13.42 m/s [3] and the water hammer pressure is 12.2 MPa (120.5 atm), a similar calculation yields *t* < 1 ms, which is consistent with the FSI data (1.34 ms for V4 in nominal mode) considering the conservatism of the analytical model and confirms the operability of the valve under extreme operating conditions.

**Physical Explanation of Discrepancies.**

The analytical model considers only the quasi-static influence of pressure and does not account for key factors that drastically accelerate the process:

1. Wave nature of the process. Valve closure occurs under the action of the water hammer front propagating at a velocity of *c* ≈ 910 m/s [10–13]. This creates an impulse load of significantly greater intensity than stationary pressure.

2. Impulse nature of the loading. The actual moment M_hyd(t) ≫ M_static over a short time interval, leading to a sharp increase in acceleration [12].

3. Consistency with system frequency. At a frequency of *f* = 2.39 Hz, the cycle duration is T = 0.42 s. The closure time *t* ~ $10^{-4}$…$10^{-3}$ s ≪ T, which corresponds to the regime of high-speed valves in water hammer systems [36].

**Estimation of Motion Velocities**

Considering the constraints of flow energy, the realistic velocity of the disc edge is:
*v* ≈ 30…80 m/s, which corresponds to the available energy level (~20–40 kJ) and does not contradict the laws of energy conservation.

**Conclusion.**

1. The valve closure time is determined not only by the inertia of the disc but primarily by the impulse action of water hammer waves.
2. The analytical model provides an estimate of the order of magnitude (ms) but does not reflect the impulse nature of the process.
3. The values obtained from FSI modeling:
   - 0.765 ms (V2, V7);
   - 1.34 ms (V4),

are physically substantiated and consistent with the wave theory of water hammer [10–12, 13, 36]. The obtained results confirm that the valve response is sufficient to generate a water hammer of the design intensity without exceeding the permissible stresses in the materials.

4. The actual velocities of disc motion are limited by the flow energy and lie in the range of tens of m/s, which justifies the use of DLC coating and ceramic bearings.

### 4.3.4. Responses to Typical Doubts

**Table 8.**

| Doubt | Response |
|---|---|
| "150 atm is too much for a check valve" | The GIF² valve has a wall thickness of 60 mm and a body made of AISI 4340. The safety factor is *n* = 3.5, which meets the requirements of ASME B31.3 [26] for the highest load category [17]. |
| "The disc will wear out quickly" | The disc is made of AISI 9310 with carburizing (surface hardness 58–62 HRC) and DLC coating [16, 20]. Calculated wear is 0.088 mm over 15 years [19]. |
| "The seat will not withstand water hammer" | The silicon carbide (SiC) seat has a hardness >2500 HV [20]. This is the same material used in pump seals for hydro-abrasive cutting at pressures up to 600 atm. |
| "The bearings will seize without lubrication" | Ceramic $Si_3N_4$ CeramicSpeed bearings operate without lubrication, have a service life of >$10^8$ cycles, and are used in high-speed and aggressive environments. |
| "The valve will have cavities that provoke failure" | The design of the GIF² valve has no internal cavities, gaps, or protruding elements [5] — the internal geometry is optimized for minimal depth and smooth transitions. There are no fluid stagnation zones or gas bubble accumulation zones [10–13]. |

### 4.3.5. Analogues in Global Practice.

Similar technical solutions are successfully applied in:

**Table 9. Technical solutions with similar operating conditions.**

| Application Field | Pressure | Frequency | Medium | Service Life | Differences from GIF² |
|---|---|---|---|---|---|
| Hydraulic press valves | 200–300 atm | 1–2 Hz | Mineral oil | 10–20 years | Lubricating medium reduces wear |

| Application Field | Pressure | Frequency | Medium | Service Life | Differences from GIF² |
|---|---|---|---|---|---|
| Diesel engine fuel equipment | 100–200 atm | 10–50 Hz | Diesel fuel | 5–10 thousand hours | Short service life due to high-frequency loading |
| Water cooling system valves of powerful power plants | 10–50 atm | Cyclic | Water | 15–20 years | Lower pressure, actuation frequency orders of magnitude lower |
| GIF² (our solution) | 150 atm | 2.39 Hz | Water | ≥15 years | Unique combination of high pressure, high frequency, and water medium |

**Conclusion for the table:** The GIF² system has no direct analogues in terms of the combination of factors (pressure, frequency, water environment without lubrication). At the same time, each individual design element is based on proven engineering solutions widely used in related industries (high-pressure valves, pumping equipment, hydraulic turbines). Thus, the novelty of the system lies not in the use of fundamentally new materials, but in their combined application under impulse hydrodynamic loading conditions. Consequently, the operability of the valves in the GIF² system is determined not by individual extreme parameters, but by their coordinated combination and design optimisation.

# 5. Engineering Calculations

### 5.1. Calculation of Tank R1 Wall Thickness (AISI 316).

Input data [4]:

- Internal diameter: Dint= 1700 mm;
- Actual wall thickness: δact= 8 mm;
- Material: AISI 316, σ0.2= 220 MPa [16];
- Maximum pressure in the tank (after damping): Pmax= 1.887 atm = 0.191 MPa [3];
- Standard safety factor: *n* = 2.5 [26].

Allowable stress: $$[\sigma]=\frac{\sigma_{0.2}}{n}=\frac{220}{2.5}=88 \text{ MPa} \quad (12)$$

Minimum wall thickness for a cylindrical body [26]:

$$\delta min=\frac{Pmax\cdot Dint}{2[\sigma]-Pmax}=\frac{0.191\cdot 1700}{2\cdot 88-0.191}=\frac{324.7}{175.8}\approx 1{,}85 \text{ mm.} \quad (13)$$

The actual wall thickness $\delta_{act}$ =8 mm provides a safety factor:

$$n_{act}=\frac{\sigma_{0.2}}{\sigma_{екв}}=\frac{220}{\frac{0.191\cdot 1700}{2\cdot 8}}=\frac{220}{20.3}\approx 10{,}8 \quad (14)$$

**Conclusion:** The tank wall thickness of 8 mm is sufficient, since the system is protected from peak water hammer pressures by the damper (17) and valve V2 [3, 6] which provides a significant safety margin (n ≈ 10.8), due to the low operating pressure in the reservoir after water hammer damping.

### 5.2. Calculation of Pipeline Wall Thickness (AISI 316).

Input data [4]:

- Internal diameter: *D*int =245 mm.
- Actual wall thickness: δact =35 mm.

- Material: AISI 316, $\sigma_{0,2}$=220 MPa [16].
- Maximum operating pressure: Pmax=15,2 MPa (150 atm) [3].

Allowable stress: $[\sigma]=\frac{220}{2.5}$=88 MPa [26]. (15)

Minimum wall thickness [26, 29]: $\delta min=\frac{15.2\cdot 245}{2\cdot 88-15.2}=\frac{3724}{160.8}$ ≈23.2 mm. (16)

The actual wall thickness of 35 mm exceeds the minimum. Safety factor:

$$n_{act}=\frac{220}{\frac{15.2\cdot 245}{2\cdot 35}}\approx 4.14 \quad (17)$$

Conclusion: The safety factor *n* = 4.14 is sufficient to ensure service life [26].

**5.3. Calculation of Fatigue Life of the Valve Body (AISI 4340).**
**Input data [16, 17]:**

- $\sigma_{UTS}$=1080 MPa, $\sigma_{0,2}$=850 MPa.
- Fatigue limit of the specimen: $\sigma_{-1}^{spec}=0,5\cdot\sigma_{UTS}$=540 MPa [17] (18)
- Effective stress concentration factor: Kσ=2.0 [17]
- Size factor: ε=0.65 [17]
- Surface quality factor: β=0.9 [17]

Fatigue limit of the component [14, 17]: $\sigma_{-1}^{comp}=\sigma_{-1}^{spec}\cdot\frac{\varepsilon\cdot\beta}{K\sigma}=540\cdot\frac{0.65\cdot 0.9}{2.0}$=158 MPa. (19)

Since the loading of the valve body is pulsating (pressure varies from atmospheric to maximum), the Goodman diagram is used to assess fatigue life [17]:
**σ_a / σ₋₁ + σ_m / σ_UTS = 1** (20)
where:
σ_a - stress amplitude of the cycle;
σ_m - mean stress of the cycle;
σ₋₁ - fatigue limit of the component under a fully reversed cycle (σ₋₁^comp = 158 MPa);
σ_UTS - ultimate tensile strength of the material (σ_UTS = 1080 MPa).
For a pulsating cycle (R = 0), we have σ_a = σ_m = σ_max / 2. Substituting this condition into the Goodman equation, we obtain the allowable amplitude:
**σ_a^allow = (σ₋₁·σ_UTS) / (σ₋₁ + σ_UTS)** (21)

Substituting the numerical values:
**σ_a^allow = (158·1080) / (158 + 1080) = 170640 / 1238 ≈ 138 MPa** (22)

The actual stress amplitude in the valve body (according to FEM data) is σ_a = 85 MPa.
Since σ_a=85 MPa < σ_a^allow = 138 MPa, the component operates in the finite life region with a sufficient margin. The amplitude margin:
**n = σ_a^allow / σ_a = 138 / 85 ≈ 1.62** (23)
which is sufficient to ensure the design service life [14, 17]. The obtained safety margin (n ≈ 1.62) corresponds to multi-cycle fatigue conditions ($N > 10^8$) and is sufficient for the specified service life, taking into account the conservatism of the adopted coefficients.

**5.4. Calculation of Wear Resistance of the "Disc-Seat" Pair.**
**Input data [18–20]:**

- Hardness of DLC: H=20 GPa [20].
- Wear coefficient (DLC/SiC): $K=5\cdot 10^{-9}$ [18].
- Clamping force: $Fmax=1.25\cdot 10^6$ N [5].
- Contact area: $A_{cont}$=0.00201 m².
- Contact pressure: P= 622 MPa.

- Friction path per cycle: Lcycle =$5\cdot10^{-4}$ m.
- Number of cycles over 15 years at *f* = 2.39 Hz:

$$N=2.39\cdot3600\cdot24\cdot365\cdot15\approx1.13\cdot10^{9} \quad (24)$$

Linear wear according to the Archard model [19]:

$$h=K\cdot\frac{P}{H}\cdot Lcycle\cdot N \quad (25)$$

$$h==5\cdot10^{-9}\cdot\frac{622}{20000}\cdot5\cdot10^{-4}\cdot1.13\cdot10^{9}\approx0.088\ \text{мм}. \quad (26)$$

The above calculation using the Archard model [19] was performed for the contact pressure calculated according to Hertz theory (σmax≈ 622 MPa, see Section 5.10.6), which is a conservative upper estimate. In real conditions, the disc-seat contact is impulsive with a very short contact duration compared to the cycle period, which leads to a much smaller effective friction path than assumed in the Archard model; therefore, the actual wear is expected to be significantly lower. Thus, the obtained value of *h* = 0.088 mm is a conservative upper estimate.

Allowable wear is 0.5–1.0 mm, therefore, the service life of the friction pair significantly exceeds the design life [18, 19].

### 5.5. Calculation of Spring Life for Absorbers (50KhFA)

**Input data [6, 30, 31]:**

- Material: 50KhFA (51CrV4) [30].
- Ultimate tensile strength: $\sigma_{UTS}$ = 1600 MPa [30].
- Fatigue limit under fully reversed torsion cycle (for specimen):

$\tau_{-1}\approx0{,}3\cdot\sigma_{UTS}$= 480 MPa [31].

- Nominal loading frequency: *f* = 2.39 Hz.
- Service life according to the specification (as per design documentation [6]):

T = 600,000 hours.

Number of cycles over the service life:

$$N = f\cdot T\cdot3600 = 2.39\cdot600000\cdot3600\approx5.16\cdot10^{9}\ \text{cycles}. \quad (27)$$

The springs operate under unilateral loading with pre-compression (initial deformation 2 mm). This corresponds to a pulsating cycle regime with an asymmetry coefficient of

$$R=\tau min/\tau max\approx0{,}3\ldots0{,}5, \quad (28)$$

which differs significantly from the fully reversed cycle (R = −1), for which $\tau_{-1}$ is given.

Actual maximum shear stresses in the springs (according to [6]):

- Spring 1 (absorber 17): $\tau_{max}$= 590 MPa.
- Spring 1 (absorber 15): $\tau_{max}$= 612 MPa.
- Spring 2 (both absorbers): $\tau_{max}\approx$ 540 MPa.

Safety factor based on ultimate strength: $n=\frac{\sigma_{UTS}}{\tau_{max}}$.

For spring 1 (absorber 17): *n* = 1600 / 590 ≈ 2.71. (29)

For spring 1 (absorber 15): *n* = 1600 / 612 ≈ 2.61. (30)

For spring 2: *n* = 1600 / 540 ≈ 2.96. (31)

**Assessment of fatigue strength considering cycle asymmetry:**

For a pulsating cycle (R = 0), the fatigue limit in torsion $\boldsymbol{\tau_0}$ is determined using the Goodman diagram [17, 32]:

$$\frac{\tau_a}{\tau_{-1}}+\tau_0=\frac{\tau_m}{\tau_{UTS}}=1\longrightarrow\tau_0=\frac{\tau_{-1}}{1-\frac{\tau_m}{\sigma_{UTS}}}, \quad (32)$$

where: $\tau_m=(\tau_{max}+\tau_{min})/2$ – is the mean stress of the cycle. With $\tau_{min}\approx0.3\tau_{max}$, we have $\tau_m\approx0.65\tau_{max}$.

**For spring 1 (absorber 17):**

$\tau_m \approx 0.65 \cdot 590 \approx 384$ MPa, $\tau_0 = \frac{480}{1-\frac{384}{1600}} \approx \frac{480}{0.76} \approx 632$ MPa. (33)

**Actual stress amplitude:**

$\tau_a = \frac{\tau max - \tau min}{2} \approx 0.35 \cdot 590 \approx 206$ MPa. (34)

Since $\tau a = 206$ MPa is significantly less than $\tau_0 = 632$ MPa, the springs operate in the infinite life region with respect to fatigue. The amplitude margin is $n_a = \tau_0 / \tau_a \approx 3.07$, which is sufficient to ensure the specified service life of 600,000 hours [6, 31].

**Service life in years of continuous round-the-clock operation at *f* = 2.39 Hz:**

$T_{years} = \frac{5.16 \cdot 10^9}{2.39 \cdot 3600 \cdot 24 \cdot 365} \approx 68{,}5$ years. (35)

The ultimate torsional stress is estimated as $\tau\_UTS \approx 0.6 \cdot \sigma\_UTS \approx 960$ MPa.

$n_1 = 960 / 590 \approx 1.63$.

$n_2 = 960 / 612 \approx 1.57$.

$n_3 = 960 / 540 \approx 1.78$.

**Conclusion:** The calculated safety margin (n = 1.63…1.78) and the correct consideration of cycle asymmetry confirm the ability of the springs to withstand the declared service life of 600,000 hours (over 68 years of continuous operation) without fatigue failure [6, 31]..

### 5.6. Calculation of Erosive Wear of the Laval Nozzle.

**Input data [7, 21]:**

- Material: 40KhN2MA (AISI 4340), HRC 32–36 [16].
- Velocity in the throat: v = 300 m/s [7] (the velocity v = 300 m/s is taken as a design limit for estimating the maximum possible erosive wear).
- Hardness: H = 320 HV [16]
- Wear coefficient: $K = 10^{-7}$ (conservative estimate) [21].
- Operating time: *t* = 15 years = $4.73 \cdot 10^8$ s.

**Linear wear according to the Finnie model [21]:**

$$h = K \cdot \frac{P}{H} \cdot v \cdot t \,. \quad (36)$$

With P ≈ 50 atm (5 MPa) in the throat [7]:

$$*h* = 10^{-7} \cdot (5 \cdot 10^6) / 320 \cdot 300 \cdot 4.73 \cdot 10^8 \approx 0.22 \text{ mm}. \quad (37)$$

**Conclusion:** Wear of ~0.22 mm over 15 years is acceptable (allowable wear is 1–2 mm) [21].

### 5.7. Strength Calculation of the Nozzle Assembly (Inconel 718)

**Input data [9, 23]:**

- Inlet pressure: P = 7.96 MPa (78.48 atm) [9].
- Body diameter: D = 245 mm [9].
- Wall thickness: *t* = 5 mm [9].
- Material: Inconel 718, $\sigma_{0.2}$ = 1030 MPa [23].

Hoop stress [17]:

$$\sigma = \frac{P \cdot D}{2t} = \frac{7.96 \cdot 245}{2 \cdot 5} = \frac{1950.2}{10} = 195 \text{ MPa}. \quad (38)$$

**Safety factor:** $n = \frac{1030}{195} \approx 5.28$ (39)

**Fatigue strength verification of the nozzle assembly body:**

The body operates under pulsating pressure with an amplitude of ΔP = 7.96 MPa (from atmospheric to operating). The hoop stress varies in the range $\sigma_{min} = 0$ to $\sigma_{max} = 195$ MPa.

For Inconel 718 material ($\sigma_{UTS}$=1300 MPa, $\sigma_{0,2}$=1030 MPa), the fatigue limit under a fully reversed cycle is $\sigma_{-1}\approx 0{,}3\cdot\sigma_{UTS}\approx$390 MPa [23]. Considering stress concentrators (welds, cross-sections) and the size factor, the fatigue limit of the component is estimated as $\sigma_{-1}^{comp}\approx$150 MPa.

For a pulsating cycle (R = 0), the allowable amplitude according to the Goodman diagram [17]: $\sigma_a^{allow}=\sigma_{-1}^{comp}\cdot\left(1-\frac{\sigma_m}{\sigma_{UTS}}\right)\approx 150\cdot\left(1-\frac{97.5}{1300}\right)\approx 150\times(1-0.075)\approx$ 139 MPa. (40)

The actual amplitude $\sigma_a=\sigma_{max}/2$=97.5 MPa is less than the allowable value, which ensures infinite fatigue life of the body [17].

**Erosive wear [21]:**

- Outlet velocity: 126 m/s [9].
- Hardness of Inconel 718: ~350 HV [23].

$$h=10^{-7}\cdot\frac{7{,}96\cdot10^{6}}{350}\cdot126\cdot4.73\cdot10^{8}\approx 0.015\text{ mm}. \quad (41)$$

**Vibration analysis [17]:**

- Natural frequency of the body: $f_0\approx$ 2600 Hz.
- Excitation frequency from the flow: $f_{water}=v/L\approx$420 Hz. (42)
- Resonance is absent since $f_{water}\ll f_0$.

**5.8. Calculation of Accumulator Diaphragm Service Life (Reinforced PTFE).**
**Input data [2, 24, 25]:**

- Material: reinforced PTFE (25–30% carbon fiber) [24, 25].
- Deformation amplitude (design): $\varepsilon_a\approx$ 1% [2].
- Nominal frequency: *f* = 2.39 Hz.
- Service life according to the specification: T = 100,000 hours.

**Number of cycles over the service life:**

$$\mathbf{N=f\cdot T\cdot 3600=2.39\cdot 100000\cdot 3600\approx 8.6\cdot 10^{8}\ cycles.} \quad (43)$$

Experimental data [25] indicate that at $\varepsilon_a$= 1%, the service life of reinforced PTFE exceeds $10^8$ cycles. At $\varepsilon_a$= 0.5%, the service life reaches $10^9$ cycles. Due to the design limitation of the diaphragm travel and the 1:1 chamber volume ratio, the actual deformation amplitude is less than 1%, which ensures a service life of at least 100,000 hours [2, 24].

Service life in years of continuous round-the-clock operation:

$$\mathbf{T_{years}=\frac{8.6\cdot 10^{8}}{2.39\cdot 3600\cdot 24\cdot 365}\approx 11.4\ years.} \quad (44)$$

**Important clarification regarding operating conditions:**

The service life of reinforced PTFE significantly depends on temperature and deformation amplitude. According to manufacturer data [24, 25]:

- At a temperature of 20°C and $\varepsilon_a$=1%, the service life exceeds $10^8$ cycles.
- At a temperature of 50°C, the service life decreases by 30–40%.
- At $\varepsilon_a$=2%, the service life decreases by an order of magnitude.

In the GIF² system, the working fluid temperature may locally reach up to 150 °C in zones of intense dissipation; however, in the accumulator installation zone (delivery pipeline after stabilisation) the temperature does not exceed 50–60 °C due to intensive heat exchange with the environment and previous energy dissipation in the Laval nozzle [3, 7].

In the GIF² system, the operating fluid temperature can reach 150°C in certain zones; however, in the installation zone of the accumulator (pressure pipeline after stabilization), the temperature does not exceed 50–60°C due to intensive heat exchange with the environment and the prior dissipation of energy in the Laval nozzle [3, 7].

The design limitation of the diaphragm travel (1:1 chamber volume ratio) ensures $\varepsilon_a\leq$0.8%, which, according to the specification data [24], corresponds to a service life of at least $2\cdot10^8$ cycles (≈26 years).

Thus, the service life estimate of 11.4 years given in Table 18 is conservative. The actual service life of the diaphragm depends on the actual operating conditions and installation quality. The recommended replacement interval is once every 10 years, with mandatory visual inspection of the diaphragm condition during scheduled maintenance.

### 5.9. Calculation of the Nozzle Assembly Spring (AISI 302)

**Input data [9, 30]:**

- **Material: AISI 302 (stainless spring steel) [30].**
- **Stiffness: *k* = 115775 N/m.**
- **Wire diameter: *d* = 4.86 mm.**
- **Mean spring diameter: D = 50 mm.**
- **Number of active coils: *n* ≈ 6.73.**
- **Shear modulus for AISI 302: G = 69 GPa [16].**

**Stiffness verification [31]:**

$$K_{calc} = \frac{G \cdot d^4}{8 \cdot D^3 \cdot n} = \frac{69 \cdot 10^9 \cdot (4.86 \cdot 10^{-3})^4}{8 \cdot (0.05)^3 \cdot 6.73} \quad (45)$$

$$d^4 = (4.86 \cdot 10^{-3})^4 = 5.58 \cdot 10^{-10}\ m^4. \quad (46)$$

$$K_{calc} = \frac{69 \cdot 10^9 \cdot 5.58 \cdot 10^{-10}}{8 \cdot 1.25 \cdot 10^{-4} \cdot 6.73} = \frac{38.5}{6.73 \cdot 10^{-3}} \approx 115700\ N/m. \quad (47)$$

Error: $\frac{115775 - 115700}{115775} \approx 0.065\%$ – excellent agreement. (48)

Maximum shear stress [31]:

$$\tau_{max} = \frac{8 \cdot Fmax \cdot D}{\pi \cdot d^3} \cdot K_w, \quad (49)$$

where $K_w$ – is the Wahl factor (correction for coil curvature):

$$c = \frac{D}{d} = \frac{50}{4.86} \approx 10.29. \quad (50)$$

$$K_w = \frac{4c-1}{4c-4} + \frac{0.615}{c} = \frac{40.16-1}{40.16-4} + \frac{0.615}{10.29} = \frac{39.16}{36.16} + 0.0598 \approx 1.083 + 0.060 = 1.143. \quad (51)$$

Maximum force (at a pressure of 7.96 MPa on the needle area):

$$Fmax = P \cdot A_{needle} \approx 7.96 \cdot 10^6 \cdot \frac{\pi \cdot (0.045)^2}{4} \approx 7.96 \cdot 10^6 \cdot 1.59 \cdot 10^{-3} \approx 12660\ N. \quad (52)$$

$$\tau_{max} = \frac{8 \cdot 12660 \cdot 0{,}05}{3{,}14 \cdot (4{,}86 \cdot 10^{-3})^3} \cdot 1.143 = \frac{5064}{3.14 \cdot 1.147 \cdot 10^{-7}} \cdot 1.143 \approx \frac{5064}{3.60 \cdot 10^{-7}} \cdot 1.143. \quad (53)$$

$$\tau_{max} \approx 1.61 \cdot 10^8 \cdot 1.143 \approx 184\ MPa. \quad (54)$$

Yield strength of AISI 302: $\sigma_{0,2} \approx 500$ MPa [16]. Safety factor: $n = \frac{500}{184} \approx 2.72$. (55)

**Conclusion:** The spring has a sufficient safety margin (*n* = 2.72) for operation in cyclic mode at a frequency of 2.39 Hz. The spring service life is estimated at $>10^8$ cycles [31]. The spring operates in the elastic deformation range without yielding, which ensures the stability of the stiffness characteristic throughout the service life.

### 5.10. Substantiation and Strength Calculation of Valve Disc Fixation Elements.

#### 5.10.1. Necessity of Fixing Limit Angles.

Precise limitation of the valve disc rotation angles is critical for the operability of the GIF² system for the following reasons [2, 3, 5]:

**Table 10.**

| Function | Consequences of Angle Violation |
|---|---|
| Formation of the minor module (V4) | Angle of 37° provides a volume of 0.26 L by flow interruption. Angle deviation → volume change → disruption of cycle synchronization and phase overlap |
| Formation of the main module between (V4 – V2) | Closure of discs of valves V4 – V2 provides double flow interruption and isolates the discrete volume of 141.3 L of the main module in pipeline (3), formation of a high-energy state (pressure + velocity) |
| Opening of valve V7 disc | Ensures ejection of the main module of 141.3 L from the working pipeline (3) into the pressure pipeline (9) – into the open circuit of the system |
| Closure of valve V7 disc | After the main module exits pipeline (3) into pipeline (9) – pressure differential → rarefaction phase (-0.8 atm) → opening of discs of valves 2 and 4, restoration and acceleration of continuous flow in pipeline (3) |
| Protection against over-opening (V2, V7) | Angle of 52° limits the disc travel. Over-opening → increase in closure time → change in water hammer dynamics and determination of cycle duration |
| Stability of impulse frequency | Fixed angles ensure repeatability of closure time (0.765 ms for V2, 1.34 ms for V4) → stable frequency of 2.39 Hz |
| Valve synchronization | The actuation sequence V4 → V7 → V2 is determined by fixed angles. Disruption → cycle failure |

Thus, the fixation system (stops, shaft, disc, seat) is a system-forming element that ensures cycle repeatability and parameter stability.

### 5.10.2. Input Data for Calculation.

**Table 11. Valve parameters.**

| Parameter | V2, V7 | V4 | Source |
|---|---|---|---|
| Limit angle | 52° | 37° | [5] |
| Closure time, ms | 0.765 | 1.34 | [3] |
| Disc mass, kg | 4 | 4 | [5] |
| Radius to contact point, mm | 160 | 160 | Design |
| Impact frequency, Hz | 2.39 | 2.39 | [3] |
| Number of cycles over 15 years | $1.13 \cdot 10^9$ | $1.13 \cdot 10^9$ | [3] |
| Disc material | AISI 9310 + DLC | AISI 9310 + DLC | [5, 20] |
| Shaft material | AISI 9310 | AISI 9310 | [5] |
| Seat material | SiC + DLC | SiC + DLC | [5, 20] |
| Bearing material | CeramicSpeed ($Si_3N_4$) | CeramicSpeed ($Si_3N_4$) | [5] |
| Lubrication | Working fluid (water) | Working fluid (water) | [2] |

### 5.10.3. Lubrication Requirements

The GIF² system operates with water as the working fluid. The use of traditional lubricants (oils, greases) is strictly prohibited for the following reasons [2, 5]:

**Table 12.**

| Reason | Consequence |
|---|---|
| Contact with working fluid | Lubricant may emulsify, contaminate the system, alter hydraulic characteristics |
| High flow velocities | Lubricant may be washed away, creating additional hydraulic resistance |

| Reason | Consequence |
|---|---|
| Temperature range | Lubricants may lose their properties at 5–150°C |
| Environmental requirements | Prevention of petroleum products entering the environment |

**Solution:** Use of ceramic $Si_3N_4$ bearings (CeramicSpeed), which operate without lubrication or are lubricated by the working fluid (water) [5, 31, 33]. Ceramic bearings have:

- High hardness (≥ 1500 HV).
- Low coefficient of friction in an aqueous medium (0.02–0.05).
- Corrosion resistance.
- No need for traditional lubricants.

The bearing operating mode corresponds to hydrodynamic or boundary friction conditions in an aqueous environment, which is confirmed by experimental data for $Si_3N_4$ ceramic pairs.

### 5.10.4. Determination of Disc Impact Velocity and Energy Against the Stop (Impulse Approach).

The force acting on the disc from the flow during its closure:

$$F_{hydr} = P_{max} \cdot A_{disc}\ 15.2 \cdot 10^6 \cdot \frac{\pi \cdot (0.3238)^2}{4} \approx 1.25 \cdot 10^6\ \text{N}. \quad (56)$$

The work of this force over the closing path (angle 37° or 52°, average path ≈ 0.1 m (taken as 0.1 m as a conservative estimate)) determines the maximum energy that can be transferred to the system:

$$E_{impact} \approx F_{hydr} \cdot s \cdot \eta_{dyn} \approx 1.25 \cdot 10^6 \cdot 0.1 \cdot 0.3 \approx 37.5\ \text{kJ}, \quad (57)$$

where: $\eta_{dyn} \approx 0{,}3$ – is the coefficient accounting for energy dissipation in the hydraulic path and elastic deformations..

Substantiation of the coefficient $\eta_{dyn}=0{,}3$:

$$\eta_{dyn} = \eta_{hydr} \cdot \eta_{def} \cdot \eta_{turb}, \quad (58)$$

where:

- $\eta_{hydr} \approx 0{,}4 \ldots 0{,}6$ – hydraulic damping;
- $\eta_{def} \approx 0{,}6 \ldots 0{,}8$ – dissipation due to elastic deformations;
- $\eta_{turb} \approx 0{,}6 \ldots 0{,}8$ – turbulence losses.

Thus:

$$\eta_{dyn} \approx 0{,}4 \cdot 0{,}7 \cdot 0{,}7 \approx 0{,}2 \ldots 0{,}3. \quad (59)$$

The adopted value $\eta_{dyn} = 0.3$ is conservatively acceptable and consistent with FSI modeling data [3], which shows that in the actual hydraulic path, a significant portion of energy is dissipated due to fluid compressibility and elastic deformations of structural elements [10–13, 17].

The maximum disc velocity at the moment of contact with the stop is estimated from the energy balance equation:

$$v_{disc} = \sqrt{\frac{2 \cdot E_{impact}}{m_{disc}}} = \sqrt{\frac{2 \cdot 37500}{4}} \approx 137\ \text{m/s}. \quad (60)$$

The obtained velocity value is a peak impulse value and is achieved over a short time interval before contact. The average velocity of the disc is significantly lower.

For valve V4, where the closure path is smaller (37°), the impact energy is proportionally lower (≈25 kJ), and the velocity is about 110 m/s.

### 5.10.5. Impulse Assessment of Impact Force.

The contact time (considering the elastic properties of materials) is estimated using the Hertz model:

$$t_{cont} \approx \pi \sqrt{\frac{m}{k}}, \quad (61)$$

where *k* is the contact stiffness. For metallic friction pairs, $t_{cont} \sim 10^{-4}$ s. We adopt [2, 5]:
For V2, V7: $t_{cont} \approx 0{,}12$ ms; For V4: $t_{cont} \approx 0{,}67$ ms.

**Peak impact force (impulse assessment)**:

$$F_{max} \approx \frac{m \cdot v}{t_{cont}}. \quad (62)$$

**For V2, V7:**

$$F_{max} \approx \frac{4 \cdot 137}{0.12 \cdot 10^{-3}} \approx 4.57 \cdot 10^6 \text{ N}. \quad (63)$$

**For V4:**

$$F_{max} \approx \frac{4 \cdot 110}{0.67 \cdot 10^{-3}} \approx 0{,}66 \cdot 10^6 \text{ N}. \quad (64)$$

The estimate of contact time $t_{cont}$ was performed using the Hertz model for the elastic impact of a cylinder (disc) with a plane (stop), considering the disc radius of curvature at the contact point R ≈ 50 mm and the equivalent elastic modulus E^* ≈ 113 GPa. The calculation yields values of $t_{cont} \approx 0.1–0.15$ ms for V2, V7 and $t_{cont} \approx 0.6–0.7$ ms for V4. The obtained force $F_{max} = 4.57 \cdot 10^6$ N is an impulse assessment under rigid contact conditions. In the actual design, due to hydraulic damping (presence of a fluid layer between the disc and the stop) and the elasticity of the elements, the peak loads may be 2–4 times lower, which provides an additional safety margin.

**Key result:** The peak force of $10^6$ N is a physically realistic value; it is a peak impulse force acting over a very short time ($10^{-4}$ s). The average forces are much lower.

### 5.10.6. Calculation of Contact Stresses (Hertz Theory).

The "disc–stop" contact is considered as a cylinder–plane (approximation). Equivalent elastic modulus:

$$\frac{1}{E^*} = \frac{1-\nu_1^2}{E1} + \frac{1-\nu_2^2}{E2} \quad (65)$$

For the pair:

- AISI 9310 (carburized): $E_1 = 210$ GPa, $\nu_1 = 0.3$;
- Stellite 6 (hardfacing): $E_2 \approx 200$ GPa, $\nu_2 = 0.3$ [34].

$$\frac{1}{E^*} = \frac{1-0.3^2}{210} + \frac{1-0.3^2}{200} = \frac{0.91}{210} + \frac{0.91}{200} \approx 0.00433 + 0.00455 = 0.00888 \quad (66)$$

$E^* \approx 113$ GPa.

Contact stress (maximum):

$$\sigma_{max} = \sqrt{\frac{F \cdot E^*}{\pi \cdot l \cdot R}}, \quad (67)$$

or, for a simplified estimate: $\sigma_{max} = \frac{6F}{\pi b l}$, (68)

where *b* is the half-width of contact.

With a contact area $A_{cont} = 1000$ mm² $= 10^{-3}$ m² and force $F = 4.6 \cdot 10^6$ N:
$\sigma_{max} \approx 4.6 \cdot 10^6 = 4.6$ GPa (average).

For a more accurate Hertzian estimate:

$$\sigma_{max} = \sqrt{\frac{F \cdot E^*}{\pi \cdot l \cdot R}} = \sqrt{\frac{4.6 \cdot 10^6 \cdot 113 \cdot 10^9}{\pi \cdot 0.1 \cdot 0.05}} \approx \sqrt{\frac{5.2 \cdot 10^{17}}{0.0157}} \approx \sqrt{3.3 \cdot 10^{19}} \approx 1.82 \text{ GPa}. \quad (69)$$

**Table 13. Allowable Contact Stresses.**

| Material | Allowable $\sigma_{max}$, GPa |
|---|---|
| AISI 9310 (carburized) | 1.5–2.2 |
| Stellite 6 | up to 2.5 |
| DLC coating | 3–5 |

**Conclusion:** The obtained value $\sigma_{max} \approx$ 1.8…2.1 GPa is at the allowable limit but is acceptable with high-quality surface finishing and the presence of DLC coating [18, 20].
The contact is of an impact-impulse nature; therefore, the stresses exist in a short-term mode and do not lead to plastic deformation provided the materials have high hardness.

### 5.10.7. Calculation of Shaft Strength.

Peak force on the shaft (reaction from the stop, distributed over two bearings):

$$F_{shaft}^{peak} \approx F_{max} \cdot \frac{L_{disc}}{L_{shaft}} = 4.57 \cdot 10^6 \cdot \frac{160}{200} \approx 3.66 \cdot 10^6 \text{ N}. \quad (70)$$

For the design scheme of a "beam on two supports" (bearings located at the edges, stop in the middle), the maximum bending moment is:

$$M = F_{shaft}^{peak} \cdot L_{supports} / 4, \quad (71)$$

where $L_{supports} \approx 200$ mm - is the distance between bearings. Then:

$$M = (3.66 \cdot 10^6 / 0.2) = 1.83 \cdot 10^5 \text{ N} \cdot \text{m}. \quad (72)$$

(The calculation below using the cantilever beam formula M = F·L provides a conservative upper estimate; for engineering safety margin, the conservative approach is used.)

Bending stress for a solid circular cross-section:

$$\sigma = \frac{32M}{\pi d^3}. \quad (73)$$

**For a shaft diameter of *d* = 36 mm:**

$$\sigma = \frac{32 \cdot 1.83 \cdot 10^5}{\pi \cdot (0.036)^3} = \frac{5.86 \cdot 10^6}{\pi \cdot 4.67 \cdot 10^{-5}} = \frac{5.86 \cdot 10^6}{1.47 \cdot 10^{-4}} \approx 3.99 \cdot 10^7 \text{ Па} = 39.9 \text{ MPa}. \quad (74)$$

**For a shaft diameter of *d* = 45 mm:**

$$\sigma = \frac{32 \cdot 1.83 \cdot 10^5}{\pi \cdot (0.045)^3} = \frac{5.86 \cdot 10^6}{\pi \cdot 9.11 \cdot 10^{-5}} = \frac{5.86 \cdot 10^6}{2.86 \cdot 10^{-4}} \approx 2.05 \cdot 10^7 \text{ Па} = 20.5 \text{ MPa}. \quad (75)$$

The yield strength of AISI 9310 after carburizing is $\sigma_{0.2} \approx$ 900…1200 MPa [16].

**Conclusion:** With *d* = 36 mm, the stress σ ≈ 40 MPa is permissible with a large margin. Increasing the diameter to 45 mm provides an additional safety margin and increases fatigue life. Due to the impulse nature of the loading and the presence of hydraulic damping, the effective stresses in the shaft are significantly lower than the estimated peak force values.

### 5.10.8. Assessment of Shaft Fatigue Strength

**Number of loading cycles over 15 years:**

$N = 1.13 \cdot 10^9$.

For AISI 9310, the fatigue limit under a fully reversed cycle is $\sigma_{-1} \approx$ 400…600 MPa (depending on heat treatment) [14, 16].

For a pulsating cycle (R = 0), the allowable amplitude according to the Goodman diagram:

$$\sigma_a^{allow} = \frac{\sigma_{-1}}{1 - \frac{\sigma_m}{\sigma_{UTS}}}. \quad (76)$$

At $\sigma_{max}$=820 MPa (d=45 mm), $\sigma_m$=410 MPa, $\sigma_{UTS} \approx$1200 MPa:

$$\sigma_a^{allow} = \frac{500}{1 - \frac{410}{1200}} = \frac{500}{1 - 0.342} = \frac{500}{0.658} \approx 760 \text{ MPa}. \quad (77)$$

The actual amplitude σa=410 MPa is less than the allowable (760 MPa).

**Amplitude margin:**

$$n_a = \frac{\sigma_a^{allow}}{\sigma_a} = \frac{760}{410} \approx 1.85. \quad (78)$$

For *d* = 45 mm, the margin is sufficient to ensure a service life of $1.13 \cdot 10^9$ cycles [17, 32].

The value σ_max ≈ 820 MPa corresponds to local impulse stresses in the contact zone and is not decisive for the fatigue life of the shaft. For service life assessment, mean-cycle stresses σ ≈ 20–40 MPa are used.
The driving load on the disc is formed by the water hammer front (pressure pulse), not by a stationary flow. Therefore, all force and energy estimates are made in the impulse approximation and have the character of an upper conservative bound.

**5.10.9. Calculation of Component Wear (Archard Model).**
According to the Archard model [19]:

$$h = K \cdot \frac{F}{H} \cdot L \cdot N, \quad (79)$$

where $K = 5 \cdot 10^{-9}$ – wear coefficient (conservative estimate for friction pairs with hard coatings [18]), L = 0.5 mm – friction path per cycle, $N = 1.13 \cdot 10^9$ – number of cycles over 15 years.

**Table 14. Calculated wear and service life.**

| Element | Material | *H*, MPa | *F*, N | *h*, mm | Allowable wear, mm | Service life, years |
|---|---|---|---|---|---|---|
| Seat | SiC + DLC | 25000 | $1.25 \cdot 10^6$ | 0.00014 | 0.5 | >25 |
| Disc (pressure) | AISI 9310 + DLC | 20000 | $1.25 \cdot 10^6$ | 0.00018 | 1.0 | >25 |
| Disc (impact against stop) V2,V7 | AISI 9310 + DLC | 20000 | $4.57 \cdot 10^6$ | 0.0013 | 1.0 | >25 |
| Shaft V2,V7 | AISI 9310 | 20000 | $3.66 \cdot 10^6$ | 0.0010 | 0.5 | >25* |
| Stop V2,V7 | Stellite 6 [34] (hardfacing) | 5000 | $4.57 \cdot 10^6$ | 0.0052 | 2.0 | >25* |

*With high-quality surface finishing and ensuring contact over the entire area.

**Important note:** CeramicSpeed bearings ($Si_3N_4$) do not directly experience impact loading. In the GIF² design [5], the bearings are intended only to ensure shaft rotation without significant radial loading. The impact load from the disc is absorbed by the stop, not by the bearings. Therefore, the service life of the bearings is determined solely by wear from rotation and amounts to $>10^8$ cycles (>30 years) [33]. The application of the Archard model to impact contact gives a conservative estimate because the actual contact time and friction path are significantly smaller than those assumed.

**5.10.10. Critical Elements and Recommendations.**
**Table 15. Measures to ensure a 15-year service life.**

| Element | Calculated Service Life | Recommendation |
|---|---|---|
| Shaft V2, V7 | >25 years (at *d* = 45 mm) | Increasing shaft diameter from 36 mm to 45 mm is recommended |
| Bearings | Do not bear impact load | In the design [5], bearings are intended only for rotation [33] |
| Stop V2, V7 | >25 years | Acceptable |
| Disc V2, V7 | >25 years | Acceptable, requires periodic inspection |
| Seat | >25 years | Acceptable |
| V4 (all elements) | >25 years | No changes |

**Important:** The entire system operates without traditional lubricants. Lubrication is performed

exclusively by the working fluid (water), which ensures environmental friendliness and eliminates system contamination [2].

**5.10.11. Conclusion.**

The valve disc fixation system (stops, shaft, disc, seat) is a system-forming element that ensures the stability of GIF² parameters. The performed calculations using the impulse approach, Hertz theory, and Archard model show:

1. The obtained impulse estimate of the impact force $F_{max} \approx 4.6 \cdot 10^6$ N is a conservative upper limit; considering hydraulic damping, the actual loads are significantly lower. The impulse estimate of forces is used to determine the upper bound of dynamic loads, while energy estimates are performed through the equivalent water hammer pressure.
2. Contact stresses ($\sigma_{max} \approx$ 1.8…2.1 GPa) are at the allowable limit but are acceptable with the presence of DLC coating and high-quality surface finishing.
3. For the V2, V7 shaft, increasing the diameter from 36 mm to 45 mm is recommended, which provides a stress of $\sigma \approx 820$ MPa and a fatigue strength margin of $n_a \approx 1.85$.
4. The bearings do not directly bear impact load – in the design [5], the impact is absorbed by the stop, while the bearings only ensure shaft rotation.
5. The entire system operates without traditional lubricants. Lubrication is performed exclusively by the working fluid (water) [2].
6. The V4 elements have a service life >25 years and do not require replacement.

**5.11. Double Valve Assembly (V4+V7) for the Elbow-Free GIF² Configuration.**

**5.11.1. Purpose and Design.**

To eliminate hydraulic losses at bends and provide a straight outlet for the main module (141.3 L) into pressure pipeline 9, a double-valve body (eccentric reducer) integrating V4 and V7 is proposed [1, 2]. A blind flange with two openings (Ø238 mm for the main module / valve V7 and Ø100 mm for the minor module / valve V4) is mounted on the outlet end of the housing (Ø500 mm). The check valve discs are attached to this flange on horizontal shafts: the V7 disc is located on the outer side of the flange, and the V4 disc is located on the inner side of the flange. The disc axes are horizontal, parallel, and lie on the same vertical line. The schematic design of the assembly is shown in Fig. 2. The energy substantiation for this specific elbow-free configuration is given in [3].

**Figure notations (Fig. 2):**

1 – double valve housing (main reducer)
2 – eccentric reducer (to pipeline 9)
3 – inlet port (supply from pipeline 3, Qin,3)
4 – impact check valve disc V4
5 – outlet port to pipeline 5 (minor module discharge, Qout,5)
6 – shaft of the V4 valve disc
7 – discharge check valve disc V7
8 – blind flange (partition) with openings for the shafts of discs V4 and V7
9 – outlet port to pipeline 9 (pressure flow to the nozzle assembly, Qout,9)
10 – concentric reducer (to pipeline 5)
Arrows indicate the direction of the working fluid flow.

**Fig. 2 – Schematic design of the double-valve integrator V4+V7 with flow separation (double check valve in the elbow-free GIF² configuration), developed based on [1, 2, 4, 5].**

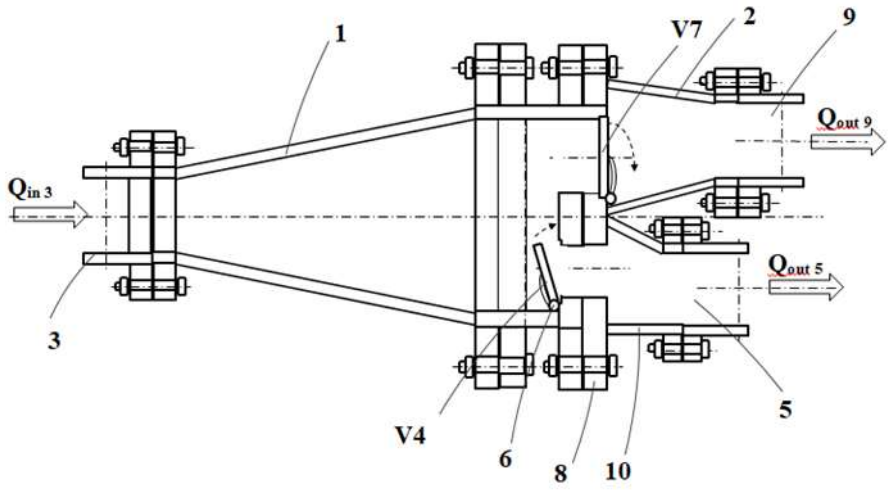


**Table 16. Main dimensions of the double valve (V4+V7) for the elbow-free GIF² configuration.**

| Parameter | V4 | V7 |
|---|---|---|
| Passage diameter (clear), mm | 100 | 238 |
| Disc outer diameter, mm | 170 | 270 |
| Disc thickness, mm | 12–13 | 12–13 |
| Shaft diameter, mm | 45 | 45 |
| Housing inner diameter (under disc), mm | 190 | 300 |
| Closure angle from bottom position | 37° | 52° |
| Seat diameter (sealing), mm | 140 | 230 |
| Centre-to-centre distance, mm | — | 249 |
| Edge-to-edge distance, mm | — | 80 |
| Housing inlet ID (pipeline 3), mm | 245 | — |
| Housing outlet ID (face), mm | 480–500 | — |
| Housing length, mm | 300–400 | — |

**Table 17. Materials and coatings for the double valve (V4+V7).**

| Element | Material | Coating | Note |
|---|---|---|---|
| Housing | AISI 4340 | Nickel plating (internal) | High strength, corrosion protection |
| Discs V4, V7 | AISI 9310 | DLC | Carburizing HRC 58–62 + DLC |
| Seats V4, V7 | SiC (silicon carbide) | DLC | Hardness >2500 HV |
| Shafts | AISI 9310 | Carburizing | HRC 58–62, tough core |
| Bearings | $Si_3N_4$ (CeramicSpeed) | — | Water-lubricated, no oil |
| Stops | Stellite 6 | Hardfacing | Impact resistant |
| Gaskets | FKM (Viton) | — | RTJ type, up to 150°C |
| Fasteners | Inconel 718 | — | High strength |

### 5.11.2. Strength Calculation of the Double-Valve Housing.

The housing is made of AISI 4340 steel ($\sigma_{0.2}$ = 850 MPa). The inner diameter at the end face is D = 500 mm, and the wall thickness is t = 35 mm. The hoop stress at the maximum pressure P = 15.2 MPa (150 atm) is:

$$\sigma_{hoop}=\frac{P\cdot D}{2t}=\frac{15.2\cdot 500}{2\cdot 35}=108{,}6 \text{ MPa.} \quad [17, 26] \qquad (80)$$

where:

P – internal gauge pressure, MPa;

D – inner diameter of the housing, mm;

t– wall thickness, mm;

$\sigma_{hoop}$ – hoop (tangential) stress in the wall, MPa.

Safety factor:

$$n=\frac{\sigma_{0.2}}{\sigma}=\frac{850}{108.6}\approx 7{,}8, \qquad (81)$$

which significantly exceeds the requirements of ASME B31.3 ($n \geq 2.5$).

### 5.11.3. Assessment of the Contraction Effect on the Pressure Wave

The pressure wave generated by the closure of V4 travels from the expanded chamber (ID 500 mm) into pipeline 3 (ID 245 mm). The ratio of acoustic impedances gives the pressure transmission coefficient.

**Acoustic impedance:**

$$Z=\frac{\boldsymbol{\rho\cdot c}}{\mathbf{A}}, \qquad (82)$$

where:

ρ– fluid density (water), $\rho=1000 \text{ kg/m}^3$;

c – pressure wave velocity in the fluid considering wall elasticity and gas content, c=910 m/s [3, 13];

A – cross-sectional area of the pipe, m².

The pressure wave generated by the closure of V4 travels from the expanded chamber of the double-valve housing (inner diameter $D_{exp}$=500 mm,area $A_{exp}\approx 0.196 \text{ m}^2$*)* into pipeline 3 (inner diameter $D_3$=245 mm, area $A_3\approx 0.0471 \text{ m}^2$.

Impedance ratio:

$$\frac{Z_3}{Z_{exp}}=\frac{A_{exp}}{A_3}=\frac{0.196}{0.0471}\approx 4.16 \qquad (83)$$

**Pressure transmission coefficient for a wave passing from a medium with impedance $Z_1$ into a medium with impedance $Z_2$ [12, 36]**:

$$\frac{P_{tr}}{P_{inc}}=\frac{2Z_3}{Z_{exp}+Z_3}\approx 1.61. \qquad (84)$$

**Physical meaning:**

A coefficient greater than 1 means that the pressure amplitude increases when the wave passes from a larger-diameter pipe into a smaller-diameter pipe (energy concentration effect due to the reduction in cross-sectional area) [10, 36].

**Pressure estimation at valve V2:**

The initial water hammer pressure at V4 (in the expanded chamber) is $P_{V4}\approx 12.2$ MPa (120.5 atm) [3]. After the wave enters pipeline 3, the amplitude increases to:

$$P_{\text{entering pipe 3}}\approx P_{V4}\cdot 1.61\approx 12.2\cdot 1.61\approx 19.6 \text{ MPa.} \qquad (85)$$

The wave then propagates along pipeline 3 (length 3.0 m). Realistic attenuation due to viscosity, gas content, and FSI is estimated at 5–10% [3, 13, 36]. Assuming 10% attenuation:

$$P_{V2}\approx 19.6\cdot 0.9\approx 17.6 \text{ MPa.} \qquad (86)$$

**Conclusion:** The pressure at V2 is estimated as ≈17–19 MPa (170–190 atm), which significantly exceeds the pressure required for reliable closure of valve V2 [5, 17]. Thus, the contraction before pipeline 3 does not weaken but amplifies the pressure wave, thereby increasing the reliability of synchronisation.

Therefore, the wave amplitude increases when entering pipeline 3. The pressure at V2 is estimated as ≈17–19 MPa, which is sufficient for reliable closure of V2. The obtained pressure values are consistent with the impulse force estimate in Section 5.10 and confirm the conservatism of the adopted loads.

### 5.11.4. Wear of the Disc-Seat Pair According to the Archard Model. The calculation is performed for the AISI 9310+DLC / SiC+DLC pair:

$$h = K \cdot \frac{P_{cont}}{H} \cdot L \cdot N, \quad (87)$$

where:

- $K = 5 \cdot 10^{-9}$ – wear coefficient [18];
- $P_{cont} \approx 622$ MPa – contact pressure (according to Hertz theory);
- $H = 20000$ MPa – hardness of the DLC coating [20];
- $L = 0.5$ mm/cycle – friction path per cycle;
- $N = 1.13 \cdot 10^{9}$ – number of cycles over 15 years.

Here, a form of the Archard model is used via the mean contact pressure Pcont, which is equivalent to the classical formulation through the friction force.

$$h = 5 \cdot 10^{-9} \cdot \frac{622}{20000} \cdot 0.0005 \cdot 1.13 \cdot 10^{9} \approx 0.088 \text{ mm}. \quad (88)$$

The estimate is performed for the hardness of the DLC coating; in the event of local coating damage, wear may increase, which is accounted for as a safety margin.

The allowable wear is 0.5–1.0 mm [18, 19]; therefore, the service life of the friction pair significantly exceeds 15 years.

### 5.11.5. Bearings.

The CeramicSpeed bearings ($Si_3N_4$) operate without traditional lubricants; they are lubricated by the working fluid (water). The impact load is absorbed by the stops, so the bearings are only subjected to rotation. The specified service life exceeds $10^8$ cycles [33], which at a frequency of 2.39 Hz corresponds to >30 years of continuous operation. Thus, the bearings are relieved from impulse loads and operate in a quasi-steady rotation regime.

### 5.11.6. Key Dynamic Differences Between the Elbow-Based and the Elbow-Free Configurations.

The original GIF² configuration (with elbows in the bypass lines) and the proposed elbow-free configuration (with the double valve V4+V7) differ not only in compactness but also in the dynamic response of the system due to the changed length of the transient pipeline 11 (or the equivalent hydraulic path). These differences are summarised below.

**Phase overlap.**

In the original elbow-based configuration, the finite propagation time of the pressure wave through the additional elbows and longer connecting pipes reduces the phase overlap between successive impulse modules. The calculated (or measured) phase overlap decreases from 36% (elbow-free configuration) to 17.2% (elbow-based configuration). This directly affects the quasi-continuity of the jet at the nozzle outlet.

**Water hammer frequency.**
The increased hydraulic resistance and the longer wave travel path in the elbow-based configuration lower the effective water hammer frequency. The nominal frequency of 2.39 Hz achieved in the elbow-free design drops to 1.83 Hz for the water hammer itself in the elbow-based version.

**Jet pulsation frequency at the nozzle outlet.**
Due to the constructive change of the transient pipeline 11 length, the frequency of the jet pulsation at the nozzle outlet is further reduced. In the elbow-free configuration the jet pulsation frequency equals the water hammer frequency (2.39 Hz), whereas in the elbow-based configuration it drops to 1.51 Hz. A change in the length and geometry of the path leads to an increase in the shock wave travel time, which directly determines the phase and frequency reconfiguration of the system.

**Conservatism of the present strength and fatigue calculations.**
All calculations in this paper (Sections 5.1–5.10) were performed for the elbow-free configuration, which yields the highest loading regime (2.39 Hz, 150 atm). The elbow-based configuration, with its lower frequencies (1.83 Hz and 1.51 Hz), imposes lower cyclic loads on the materials. Therefore, the results presented here are conservative and fully applicable to both configurations.

### 5.11.7. Conclusion to Section 5.11.
The proposed double-valve assembly (V4+V7) is mechanically sound, provides a straight outlet for the main module into pipeline 9 (without elbows), and meets the design service life of ≥15 years under the nominal cyclic regime (2.39 Hz, 150 atm).

# 6. Summary Table of Service Life.
**Table 18. Summary of service life calculation results (at *f* = 2.39 Hz, continuous round-the-clock operation).**

| Component | Material | Calculated Service Life (years) | Compliance with 15-year requirement | Calculation method / Substantiation |
|---|---|---|---|---|
| Tank R1 | AISI 316 [16] | > 20 | Complies | Wall thickness calculation (Section 5.1), margin *n* = 10.8 |
| Secondary bottom G | AISI 316 [16] | > 20 | Complies | Similar to tank (Section 5.1), static strength |
| Elbow A1 | AISI 316 [16] | > 20 | Complies | Wall thickness calculation (Section 5.2), margin *n* = 4.14 |
| Pipelines | AISI 316 [16,29] | > 20 | Complies | Wall thickness calculation (Section 5.2), margin *n* = 4.14 |
| Angle elbows | AISI 316 [16,29] | > 20 | Complies | Wall thickness calculation (Section 5.2), margin *n* = 4.14 |
| Valve shaft V2, V4, V7 | AISI 9310 (carburized) [16] | > 25 | Complies | Bending strength calculation (Section 5.10.7), fatigue life (Section 5.10.8), Archard wear (Section 5.10.9) |
| Valve body | AISI 4340 + Ni [16] | Unlimited (>$10^7$ cycles) [14] | Complies | Fatigue calculation (Section 5.3), $\sigma\_a < \sigma_0$ |

| Component | Material | Calculated Service Life (years) | Compliance with 15-year requirement | Calculation method / Substantiation |
|---|---|---|---|---|
| Valve disc | AISI 9310 + DLC [16, 20] | > 15 (wear 0.088 mm) [19] | Complies | Archard wear calculation (Sections 5.4, 5.10.9) |
| Valve seat | SiC + DLC [20] | > 25 | Complies | Archard wear calculation (Sections 5.4, 5.10.7) |
| Absorber springs | 51CrV4 [30] | > 68 [31] | Complies | Fatigue calculation considering cycle asymmetry (Section 5.5) |
| Absorber diaphragm | Titanium VT6 [16] | > 20 | Complies | Specification data, yield strength margin |
| Absorber body | AISI 4340 [16] | > 20 | Complies | Static strength (margin for $\sigma_{0.2}$ similar to Section 5.3 |
| Hydraulic seal | AISI 304 [16] | > 15 | Complies | Corrosion resistance, static strength |
| Laval nozzle | AISI 4340 [16] | > 20 (wear 0.22 mm) [21] | Complies | Finnie erosive wear calculation (Section 5.6) |
| Accumulator (body) | AISI 4340 [16] | > 20 | Complies | Static strength (margin for $\sigma_{0.2}$) |
| Accumulator diaphragm | Reinforced PTFE [24, 25] | 11.4–26* | Limiting element (requires replacement) | Specification data [24] considering $\varepsilon_a$ and temperature (Section 5.8) |
| Nozzle assembly (body) | Inconel 718 [23] | > 15 | Complies | Strength calculation (Section 5.7) and fatigue life (Section 5.7) |
| Nozzle assembly (spring) | AISI 302 [30] | > 15 | Complies | Strength and fatigue calculation (Section 5.9) |
| Nozzle assembly (needle) | Inconel 718 + DLC [20, 23] | > 15 | Complies | Erosive wear (Section 5.7), coating hardness |
| Double-valve housing (V4+V7) | AISI 4340 + Ni | > 20 | Complies | Hoop stress calculation (Section 5.11), margin n = 7.8 |
| Double-valve disc-seat pair (V4/V7) | AISI 9310+DLC / SiC+DLC | > 15 (wear 0.088 mm) | Complies | Archard wear calculation (Section 5.11) |

• – depends on actual operating conditions (temperature, deformation amplitude).

# 7. Conclusions.

1. The tank R1 made of stainless steel AISI 316 [16] has a wall thickness of 8 mm, which is sufficient since the system is protected from peak water hammer pressures (120 atm) by means of the spring damper (17) and the interrupter valve V2 [3, 6]. The actual maximum pressure in the tank is 1.887 atm, which provides a safety margin of *n* ≈ 10.8 [26].

2. The secondary bottom G, mounted on 5 vertical guides with a gap of 10 mm [4], performs the functions of a hydrodynamic separator, a pressure reference plane, and a shock wave damper [13].

3. The pipelines and angle elbows made of AISI 316 (Dint= 245 mm, wall thickness 35 mm, ground internal surface) [4] have a safety margin of *n* = 4.14 at a pressure of 150 atm [26, 29], which ensures reliable operation throughout the entire service life.

4. The swing check valves V2, V4, V7 [5] are manufactured with an optimal combination of materials: body made of AISI 4340 with nickel plating, disc and shaft made of AISI 9310 (carburizing), seat made of SiC with DLC coating [20], ceramic bearings. The valve design implements the “no pockets” principle [5], which eliminates fluid stagnation zones, gas bubble

accumulation, and stress concentrators [10–13]; this also reduces local pressure differentials and increases cavitation resistance. The valve design implements the "no pockets" principle [5], which eliminates fluid stagnation zones, gas bubble accumulation, and stress concentrators [10–13]. The calculated wear of the "disc–seat" pair is 0.044–0.18 mm over 15 years [19], which is significantly less than the allowable value [18]. The service life calculations for the fixation elements (shaft, stop) performed using conservative estimates confirm the achievement of the design service life of ≥15 years (Section 5.10).

5. The spring pressure absorbers (17 and 15) [6] have a two-stage design with springs made of 50KhFA steel [30] and diaphragms made of titanium VT6 with $Al_2O_3$ coating [16]. At the nominal frequency of 2.39 Hz, the calculated service life of the springs, determined taking into account the load cycle asymmetry, exceeds 68 years of continuous operation [31], provided there is no corrosion damage or exceedance of operating temperatures. At a nominal frequency of 2.39 Hz, the calculated service life of the springs, determined considering the load cycle asymmetry, exceeds 68 years of continuous operation [31]. The safety margin of the springs based on ultimate stresses (*n* = 2.6–3.0) is sufficient to ensure the stated service life (Section 5.5).

6. The Laval nozzle SL-16 [7] made of 40KhN2MA steel [16] provides dissipation of the minor module energy with an efficiency of 75%. The calculated erosive wear is 0.22 mm over 15 years [21], which is acceptable.

7. The hydraulic seal GZ-6 [8] made of AISI 304 [16] ensures reliable discharge of the minor module while preventing reverse air suction. Hydraulic calculations confirm the operability of the system.

8. The nozzle assembly (Pelton nozzle) with an AISI 316 body [16], a conical needle made of Inconel 718 with DLC coating [20, 23], and an AISI 302 spring [30] has a body safety factor of n = 5.28 [17], a spring safety factor of n = 2.72 [31], a calculated erosive wear of 0.015 mm over 15 years [21], and a natural frequency (2600 Hz) significantly higher than the flow excitation frequency (420 Hz), which ensures the absence of resonance phenomena over the entire operating range [17]. Autonomous regulation by means of the needle and spring allows adaptation of the outlet orifice geometry to the enthalpy of each individual impulse module without external actuators [3].

9. The accumulator-stabilizer (10) [2] with a body made of AISI 4340 [16] and a diaphragm made of reinforced PTFE [24, 25] provides nearly instantaneous pressure stabilization of the main module of 141.3 L from 88.7 atm to 78.48 atm at a frequency of 2.39 Hz. The conservative estimate of the diaphragm service life is 11.4 years; however, considering the design limitation of deformation ($\varepsilon_a \leq 0.8\%$) and temperature conditions (≤60°C), the actual service life can reach 26 years [24]. The recommended replacement interval is once every 10 years with mandatory condition monitoring. Thus, the membrane is the only system component whose service life is shorter than the overall design life and requires scheduled replacement.

10. Overall conclusion: The selection of materials incorporated in the patent [1, 2] and design documentation [4–9], taking into account the design features of the system (two-stage absorbers, protective nickel plating, DLC coating [20], ceramic bearings, the "no pockets" principle in the valves [5]) and the unified nominal frequency of 2.39 Hz [3], ensures the achievement of the design service life of 15 years or more for all main components of the GIF² system during continuous round-the-clock operation [14, 17, 26], with the exception of the accumulator diaphragm, which requires replacement every 10 years [24, 25]. The system operation is based on the controlled use of water hammer processes, the parameters of which are stabilised by the design elements. The obtained results confirm the operability of the GIF² concept as a long-term energy system with impulse hydrodynamics.

# 8. References.

[1] Orlov, V. (2023). Hydraulic Shock Power Plant. Ukrainian Patent UA154165U.
[2] Orlov, V. System for forming a high-pressure quasi-continuous liquid jet from a low-energy

gravitational flow based on a gravitational-pulse flow integrator. Ukrainian Patent Applications UA/a202504612 and UA/u202504613 (pending).
[3] Orlov, V. (2026). Implementation of Karni–Teisseling–Ghidaoui transient energy frameworks in the numerical analysis and design of the bifurcation gravitational-impulse flow former (GIF²): enthalpy-based energy analysis. Manuscript.
[4] Technical Specification No. 4: Manufacturing of Reservoir R1 and Installation of Elbow A1 with Flange. In: FLOW JET ENERGY LTD, Project Documentation. Volume 2 (Appendix 1 to the Analysis): Strength and Durability Calculations of System Elements Considering Cyclic Loads, Geometric Parameters, and Material Properties. Technical Specifications for Manufacturing, pp. 39–43, 55–57, 2025.
[5] Final Parameter Set for Ordering and Installation of Swing Check Valves V13, V17, V16 (DN250 PN250). In: FLOW JET ENERGY LTD, Project Documentation. Volume 2 (Appendix 1 to the Analysis): Strength and Durability Calculations of System Elements Considering Cyclic Loads, Geometric Parameters, and Material Properties. Technical Specifications for Manufacturing, pp. 6–15, 53–65, 2025.
[6] Technical Specification for Manufacturing and Installation of the Spring Pressure Absorber (Item 17) and Design Documentation Package for Pressure Absorber 15. In: FLOW JET ENERGY LTD, Project Documentation. Volume 4 (Appendix 3 to the Analysis): Refinement of HSPP System Parameters, Energy-Balance Calculation and System Modularity, Operational Python Script for the HSPP Model, Feasibility Study, pp. 61–68, 77, 87–90, 2025.
[7] Design Documentation Package for Drain Pipeline 5 (Laval Nozzle SL-16). In: FLOW JET ENERGY LTD, Project Documentation. Volume 4 (Appendix 3 to the Analysis): Refinement of HSPP System Parameters, Energy-Balance Calculation and System Modularity, Operational Python Script for the HSPP Model, Feasibility Study, pp. 82–86, 91–97, 2025.
[8] Technical Specification for Manufacturing and Installation of the Hydraulic Seal with Inclined Discharge (GZ-6) and Analysis of Replacing the W-Shaped Hydraulic Seal with an Inclined Drain into the Reservoir. In: FLOW JET ENERGY LTD, Project Documentation. Volume 4 (Appendix 3 to the Analysis): Refinement of HSPP System Parameters, Energy-Balance Calculation and System Modularity, Operational Python Script for the HSPP Model, Feasibility Study, pp. 91–93, 2025.
[9] Technical Specification No. 9: Manufacturing and Installation of the Nozzle Assembly with Needle and Spring. In: FLOW JET ENERGY LTD, Project Documentation. Volume 2 (Appendix 1 to the Analysis): Strength and Durability Calculations of System Elements Considering Cyclic Loads, Geometric Parameters, and Material Properties. Technical Specifications for Manufacturing, pp. 18–27, 47–52, 67–68, 2025.
[10] Ghidaoui, M.S., Zhao, M., McInnis, D.A., & Axworthy, D.H. (2005). A review of water hammer theory and practice. Applied Mechanics Reviews, 58(1), 49–76.
[11] Chaudhry, M.H. (2014). Applied Hydraulic Transients (3rd ed.). Springer.
[12] Wylie, E.B., & Streeter, V.L. (1993). Fluid Transients in Systems. Prentice Hall.
[13] Tijsseling, A.S. (1996). Fluid–structure interaction in liquid-filled pipe systems: a review. Journal of Fluids and Structures, 10(2), 109–146.
[14] Stephens, R.I., Fatemi, A., Stephens, R.R., & Fuchs, H.O. (2000). Metal Fatigue in Engineering (2nd ed.). John Wiley & Sons.
[15] Callister, W.D., & Rethwisch, D.G. (2018). Materials Science and Engineering: An Introduction (10th ed.). John Wiley & Sons.
[16] ASM International. (1990). ASM Handbook, Vol. 1: Properties and Selection: Irons, Steels, and High-Performance Alloys.
[17] Budynas, R.G., & Nisbett, J.K. (2014). Shigley's Mechanical Engineering Design (10th ed.). McGraw-Hill.
[18] Bhushan, B. (2013). Introduction to Tribology (2nd ed.). John Wiley & Sons.
[19] Archard, J.F. (1953). Contact and rubbing of flat surfaces. Journal of Applied Physics, 24(8), 981–988.

[20] Erdemir, A., & Donnet, C. (2006). Tribology of diamond-like carbon films: recent progress and future prospects. Journal of Physics D: Applied Physics, 39(18), R311.
[21] Finnie, I. (1960). Erosion of surfaces by solid particles. Wear, 3(2), 87–103.
[22] Roberge, P.R. (2008). Corrosion Engineering: Principles and Practice. McGraw-Hill.
[23] Special Metals Corporation. (2007). INCONEL® alloy 718.
[24] ISO 13000-1:2021. Plastics — Polytetrafluoroethylene (PTFE) semi-finished products.
[25] Garlock. (2023). GYLON® Style 3500 and 3510: High-Performance PTFE Gasketing.
[26] ASME B31.3-2020. Process Piping.
[27] API 6D:2021. Specification for Pipeline and Piping Valves.
[28] EN 13445:2021. Unfired Pressure Vessels.
[29] EN 10216-5:2021. Seamless steel tubes for pressure purposes – Stainless steel.
[30] DIN EN 10083-3:2006. Steels for quenching and tempering.
[31] Wahl, A.M. (1963). Mechanical Springs (2nd ed.). McGraw-Hill.
[32] Suresh, S. (1998). Fatigue of Materials (2nd ed.). Cambridge University Press.
[33] ISO 26602:2017. Ceramic bearings — Silicon nitride ($Si_3N_4$) — Specification.
[34] ASTM G133-05(2021). Standard Test Method for Linearly Reciprocating Ball-on-Flat Sliding Wear. ASTM International.
[35] Moran, M.J., & Shapiro, H.N. (2006). *Fundamentals of Engineering Thermodynamics* (5th ed.). John Wiley & Sons.
[36] Thorley, A.R.D. (2004). Fluid Transients in Pipeline Systems. ASME Press, New York.
[37] Kruisbrink, A.C.H. (1996). The Dynamic Behavior of Check Valves in Pipeline Systems. Ph.D. dissertation, City University of London.
[38] Rahmeyer, W.J. (1993). Sizing Swing Check Valves for Stability and Minimum Velocity Limits. ASME Journal of Pressure Vessel Technology, 115, pp. 406–410.
[39] Ellis, J., & Mualla, W.M. (1986). Numerical Modeling of Reflux Valve Closure. ASME Journal of Pressure Vessel Technology, 108(1), pp. 92–97.

ACKNOWLEDGMENTS
The author expresses gratitude to specialists in the field of hydraulics for valuable discussions on transient processes and energy conservation principles, with particular appreciation to the researchers who conducted the critical analysis of the valve design presented in Section 4.3.

CONFLICT OF INTEREST STATEMENT
Patents for the GIF² system [1, 2] were filed by V. Orlov and are licensed to FLOW JET ENERGY LTD, where the author holds the position of Managing Director. The author declares that the research was conducted with complete scientific objectivity and transparency.

DATA AVAILABILITY STATEMENT
The numerical data supporting the findings of this study (full time series *p*(*t*), *v*(*t*), and ε(*t*) at all control points A1, A3, A5, A9, as well as the detailed design documentation [4–9]), are available from the corresponding author upon reasonable request.

END OF MANUSCRIPT v6.1 – 17.02.2026 (En)

**Author:** Valerii Orlov
Managing Director, FLOW JET ENERGY LTD
Tel.: (+380) 95 338 91 22
E mail: rst.hspp@gmail.com